The Hypoxia-regulated Ectonucleotidase CD73 is a Host Determinant of HIV Latency

Hannah S. Sperber[1,2,3,6], Kyle A. Raymond[1,3], Mohamed S. Bouzidi[1,3], Tongcui Ma[3,4], Silvana Valdebenito[5], Eliseo Eugenin[5], Nadia R. Roan[3,4], Steven G. Deeks[3], Sandra Winning[7], Joachim Fandrey[7], Roland Schwarzer[6*], Satish K. Pillai[1,3*]

1. Vitalant Research Institute, San Francisco, CA, United States of America

2. Free University of Berlin, Institute of Biochemistry, Berlin, Germany

3. University of California, San Francisco, CA, United States of America

4. Gladstone Institutes, San Francisco, CA, United States of America

5. The University of Texas Medical Branch, Galveston, TX, United States of America

6. University Hospital Essen, Institute for Translational HIV Research, Essen, Germany

7. University of Duisburg-Essen, Institute for Physiology, Essen, Germany

*Correspondence: satish.pillai@ucsf.edu, Roland-Schwarzer@gmx.de

SUMMARY

Deciphering the mechanisms underlying viral persistence is critical to achieving a cure for HIV infection. We implemented a systems approach to discover molecular signatures of HIV latently-infected CD4+ T cells, identifying the immunosuppressive, adenosine-producing ectonucleotidase CD73 as a key surface marker of latent cells. Hypoxic conditioning, reflecting the lymphoid tissue microenvironment, increased the frequency of CD73+ CD4+ T cells and promoted HIV latency. Transcriptomic profiles of CD73+ CD4+ T cells favored viral quiescence, immune evasion, and cell survival. CD73+ CD4+ T cells were capable of harboring a functional HIV reservoir and reinitiating productive infection *ex vivo*. CD73 or adenosine receptor blockade facilitated latent HIV reactivation *in vitro*, mechanistically linking adenosine signaling to viral quiescence. Finally, tissue imaging of lymph nodes from HIV-infected individuals on antiretroviral therapy revealed spatial association between CD73 expression and HIV persistence *in vivo*. Our findings warrant development of HIV cure strategies targeting the hypoxia-CD73-adenosine axis.

KEYWORDS

HIV, persistence, latency, reservoir, eradication, CD73, CD39, IL8, adenosine, hypoxia, lymphoid tissues, HIV cure.

INTRODUCTION

In recent decades, remarkable scientific and biomedical advances have turned the tides in the ongoing fight against the global human immunodeficiency virus (HIV) epidemic. However, current therapeutic regimens fail to completely eradicate HIV due to the persistence of latently-infected cells[1]. These viral reservoirs are established very early during infection, remain invisible to the host's immune system, and persevere for decades despite effective antiretroviral therapy (ART)[2–4]. Although latently-infected cells are extremely rare[5–7], they are able to reinvigorate spreading infection rapidly, and people living with HIV (PLWH) almost inevitably experience viral rebound within weeks of a treatment interruption[2,8].

The identification of reliable biomarkers or unique gene expression patterns in HIV latently-infected cells are key goals of current HIV research efforts. Such factors could contribute to the development of a cure by: 1) refining and broadening our understanding of HIV latency mechanisms and the biology of viral persistence, 2) enabling accurate quantification of viral reservoirs to assess viral burden and efficacy of therapeutic interventions, and 3) providing potential therapeutic targets to specifically eliminate viral sanctuaries. However, the heterogenous and dynamic nature of the viral reservoir greatly complicates this endeavor[9].

Viral reservoirs are found in a variety of anatomical sites and cell types. Infected CD4+ T cells arguably constitute the most important HIV reservoir[10], and within this highly diverse cell lineage, the expression of several cellular factors is associated with increased levels of integrated proviral DNA[11]. This includes immune checkpoint molecules such as programmed cell death protein 1 (PD-1), cytotoxic T-lymphocyte-associated protein 4 (CTLA-4), lymphocyte-activation gene 3 (LAG-3), and T cell immunoreceptor with Ig and ITIM domains (TIGIT)[9,12,13]. Moreover, expression levels of CD2 in CD4+ T cells were reported to identify HIV latently-infected cells[14], while CD20[15] and CD30[16] expressing CD4+ T cells were found to be specifically enriched for HIV RNA. In 2017, Descours et al.[17] proposed CD32a as

29 a viral reservoir marker and described an unprecedented 1000-fold enrichment in
30 HIV DNA in CD32a+ cells as compared to CD32a- CD4+ T cells. However, this
31 finding has been repeatedly challenged in subsequent studies and incited a
32 controversial discussion[18–25].

33 In the present study, we sought to provide a better understanding of the
34 phenotypic nature of latently infected CD4+ T cells and the mechanisms involved
35 in the establishment and maintenance of HIV reservoirs. To address this aim, we
36 utilized a dual-reporter HIV construct that enables isolation and purification of
37 uninfected, productively-infected, and latently-infected primary CD4+ T cells by
38 flow cytometry[26,27]. We then characterized each of these purified cell populations
39 using systems approaches to obtain comprehensive gene and protein expression
40 profiles of HIV latently-infected cells. Observed molecular signatures of latency
41 were validated using *ex vivo* mechanistic experiments as well as profiling of tissue
42 samples from HIV-infected individuals on suppressive ART. Our data reveal a novel
43 mechanism of HIV latency establishment and maintenance, identifying the
44 hypoxia-CD73-adenosine signaling axis as a key target for therapeutic intervention
45 and diagnostic evaluation in the setting of HIV cure.

46

47 **RESULTS**

48 **Sorting of HIV_{DFII}-infected primary CD4+T cells enables isolation of latently-**
49 **infected cells.** Profiling of HIV latently-infected cells has been greatly impeded by
50 their extremely low frequencies *in vivo* in HIV-infected individuals, as well as the
51 lack of an established marker enabling purification of latent cells for downstream
52 characterization. To characterize latent HIV reservoir cells, we utilized a modified
53 version of the HIV Duo-Fluo II (HIV_{DFII}) single round, recombinant HIV dual-reporter
54 virus (Figure S1A). To achieve sufficient infection frequencies, we first activated
55 blood-derived primary CD4+T cells obtained from six healthy donors *in vitro* via
56 αCD3/αCD28 bead stimulation and infected them with HIV_{DFII} via spinoculation
57 (Figure S1B-D). Four days post infection (p.i.), productively- and latently-infected,
58 as well as uninfected cells were purified by fluorescence activated cell sorting
59 (FACS, Figure 1A). Expectedly[27], low frequencies of latently-infected cells were
60 established in all donors, whereas uninfected and productively-infected cells could
61 be rapidly collected by FACS in large numbers (Figure 1B and C). After testing the
62 sorted samples for sufficient enrichment of the desired cell populations (Figure
63 S1E), we subjected them, together with a panel of control specimens (untreated
64 samples; unstimulated, infected cells; and stimulated cells without HIV_{DFII} infection)
65 to downstream analysis using systems approaches (Figure 1A). All samples were
66 characterized using mass cytometry by time of flight (CyTOF), measuring 40 surface
67 proteins to provide immunophenotypic profiles at the single cell level. In parallel,
68 we applied NanoString hybridization and fluorescence-based digital counting
69 technology allowing for simultaneous detection of 770 mRNA and 30 protein
70 targets.

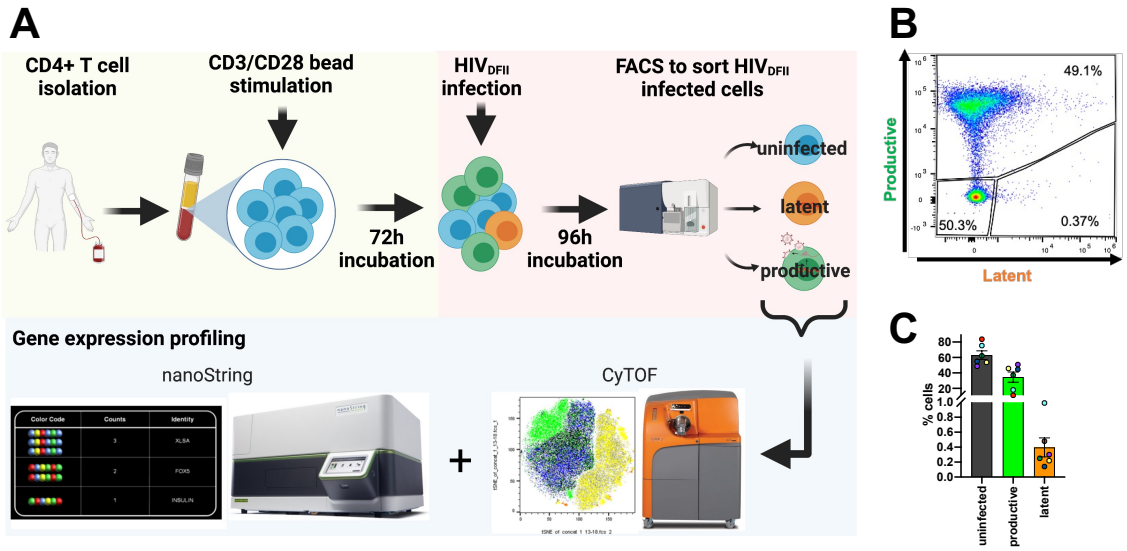

Figure 1: Isolation of latently-infected primary CD4+ T cells using the dual-reporter virus HIV_{DFII}. (A) Experimental workflow: Blood-derived primary CD4+ T cells were isolated from six healthy donors and stimulated *in vitro* with αCD3/αCD28 beads for three days. Cells were then infected with HIV_{DFII} and subjected to FACS 4 days post infection. (B) Representative gating for FACS of productively-infected, latently-infected, and uninfected CD4+ T cells. All samples were pre-gated for live, single cells. (C) Bar graph represents the frequencies of infected cells in all six donors. Colored dots indicate individual donors. Error bars show standard error of the mean (SEM).

Latently-infected cells are phenotypically diverse and include T_{regs} and Tfh cells. First, to establish an in-depth analysis of the phenotypic features of latently-infected cells, we implemented CyTOF, simultaneously quantifying the expression levels of 40 different proteins with single-cell resolution. Our labeling panel comprised T cell lineage and differentiation markers, activation markers, homing receptors, and several proteins that were described previously in the context of HIV latency[9,28,29] (Table S1). We performed extensive high dimensional analysis and generated t-distributed stochastic neighbor embedding (tSNE) plots to visualize the data and assess specific T cell subsets and population phenotypes. Across all donors, we identified latent cells in various T cell compartments, including central memory (Tcm, CD45RO+CD45RA-CCR7+CD27+), follicular helper (Tfh, CD45RO+CD45RA-PD1+CXCR5+), regulatory (Treg, CD45RO+CD45RA-CD127-CD25+), and to a lesser extent, naïve (CD45RO-CDRA+CCR7+) T cells (Figure 2).

Although memory CD4+ T cell subset frequencies exhibited variability between donors and no significant associations with latency were identified, Treg cells were most commonly represented in latent cell populations. Interestingly, CD30, a previously reported marker of transcriptionally-active reservoir cells[16], was expressed on a subset of latent cells in all analyzed donors (Figure 2).

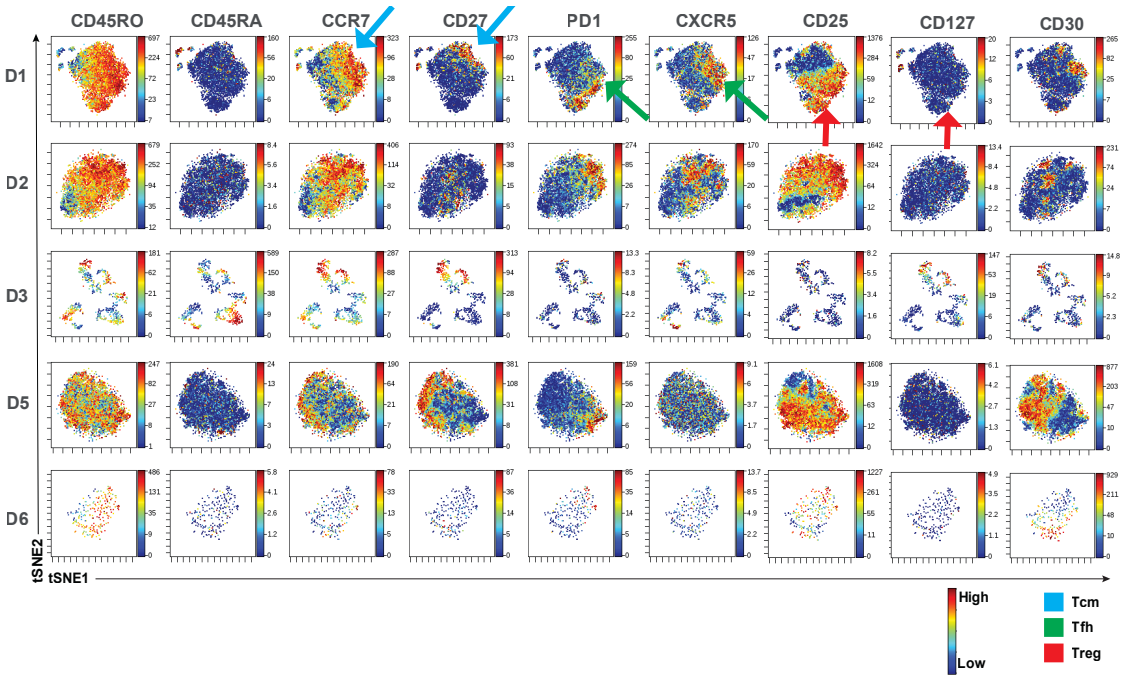

Figure 2: Multiple T cell subsets including T_{regs} are represented among HIV latently-infected cells. (A) Shown are tSNE plots of CyTOF data describing sorted latent cells from each of 5 donors (D1-D6); each donor is analyzed within its own tSNE space. tSNEs are color-coded according to expression levels of the antigen listed at the top (with red corresponding to highest expression, and blue the lowest). Most cells exhibited a memory phenotype, defined by high levels of CD45RO and low levels of CD45RA expression (first two columns). Latent cells exhibited phenotypic features of Tcm cells (CCR7+CD27+), Tfh cells (PD1+CXCR5), and T_{regs} (CD25+CD127-). Latent cells expressing CD30 (last column), a previously-described marker of reservoir cells, were observed in all donors. Areas of the tSNE corresponding to these three cell subsets are highlighted by the blue, green, and red arrows, respectively, for D1.

NanoString analysis reveals unique features of latently-infected cells that promote viral quiescence and cell survivorship. We next obtained high-dimensional NanoString data to comprehensively characterize gene and protein expression patterns of latent cells. Our initial unsupervised clustering analysis

111 revealed that donor effects dominated expression patterns (Figure 3A, see
112 dendrogram). Importantly, despite substantial donor effects, we observed that
113 expression patterns in uninfected and productively-infected cells within each
114 donor clustered with respect to latent cells, suggesting that latently-infected cells
115 exhibited distinct expression signatures (Figure 3A, see dendrogram).

116 Expression data were then adjusted for confounding donor effects for downstream
117 analyses. Subsequently, we examined changes in regulatory and signaling
118 pathways in latent cells based on undirected and directed global significance
119 scores (Figure 3B). The 'Antigen Processing', 'Adhesion', 'Pathogen Defense', and
120 'Interleukins' pathways were the most significantly modulated pathways in the
121 latent compartment. The upregulation of 'Interleukins' and 'Pathogen Defense' in
122 latently-infected cells likely reflects intracellular signaling cascades that antagonize
123 productive infection. The suppression of 'Antigen Processing' in latent cells
124 indicates the ability to evade host immunity, a pro-survival effect that could enforce
125 viral persistence. This observation is in line with previous studies reporting that HIV
126 actively subverts antigen presentation pathways[30,31].

127 Next, overall target expression in the sorted samples was assessed by differential
128 expression analysis (DE, Figure 3C). Comparison of uninfected and latently-infected
129 cells revealed 16 differentially expressed targets (adjusted p-value < 0.1), two of
130 which were identified at the protein level: HLA-DRA protein was downregulated,
131 and NT5E (CD73) protein was upregulated on the surface of latent cells. DE analysis
132 of productively- and latently-infected cells resulted in 36 significant hits (adjusted
133 p-value < 0.1), including cell-surface CD4 protein and CD73 protein. CD4 protein
134 was significantly downregulated in productively-infected cells (as expected in the
135 setting of viral expression), and CD73 protein was again upregulated in latent cells.

136 Overlapping both individual DE analyses revealed 27 targets that were uniquely
137 modulated in latent infection (p-value < 0.05, Figure 3D) with respect to both

138 productively-infected and uninfected cells. These targets comprised CD2 mRNA, a
139 checkpoint molecule which was reported previously as a surrogate marker for HIV
140 reservoirs[14], and interestingly, CD73 as only differentially-expressed protein (Table
141 S2). The list further included three mRNAs encoding transcription factors, six
142 encoding cytokines, and 11 encoding surface proteins. Among these, *NFKBIA* (NF-
143 κB Inhibitor Alpha) mRNA, which encodes a master inhibitor of the transcription
144 factor NF-κB[32], a crucial transcription factor of HIV[33,34], was significantly
145 upregulated in latent cells. In addition, *CASP1* mRNA was significantly
146 downregulated in latently-infected cells. CASP1 (Caspase-1) is a key regulator of
147 pyroptotic cell death, a highly inflammatory process that has been reported to be
148 a major determinant of HIV pathogenesis and a potent driver of virus-dependent
149 CD4+ T cell depletion[35].

150 The relationship between molecular markers of HIV latently-infected cells was then
151 investigated by utilizing the open-source software Cytoscape to generate a
152 detailed protein-protein interaction network (Figure 3E). Interestingly, all factors
153 associated with HIV latency in our analyses were members of a single, established
154 protein interaction complex. The chemotactic factor IL8 (or CXCL8) was found to
155 have the highest number of immediate connections (17 first neighbors), followed
156 by the transcription factor STAT1 (Signal Transducer and Activator Of Transcription
157 1, 15 first neighbors) and the cytokine CSF2 (Colony Stimulating Factor 2, 15 first
158 neighbors).

159 **Three key members of the adenosinergic pathway, IL8, CD39, and CD73, are**
160 **differentially expressed in latent cells.** To deepen our characterization of HIV
161 latently-infected cells, we additionally considered non-activated (no exposure to
162 αCD3/αCD28-stimulating beads) and non-virus-exposed cell populations in our
163 NanoString analyses. Inclusion of these comparators more faithfully emulates the
164 *in vivo* landscape in ART-suppressed individuals where the majority of CD4+ T cells
165 are likely in a resting state and have not encountered HIV.

166 Next, DE analysis was implemented to compare latent cells in a pairwise fashion to
167 all other cellular populations (Figure 3F). The pairwise DE analyses were then
168 overlaid to identify genes that were uniquely regulated in latently-infected cells
169 (Figure 3G). We identified three targets that were significantly modulated with
170 respect to all other comparator groups: IL8 mRNA, CD39 mRNA, and CD73 protein
171 (a key marker revealed in our previous analyses) (Figure 3H). These three factors
172 are known to be mechanistically connected through the adenosine signaling
173 pathway, and our observed induction of IL-8 gene expression in latently-infected
174 cells (Figure 3H) potentially reflects ADORA2B stimulation[36–40].

175 **CD73 is highly expressed on a subset of PD-1, CD39, CD49d and CD2-positive**
176 **cells.** CD39 and CD73 are surface proteins and thus could serve as convenient
177 indicators of latent reservoir cells. We therefore sought to examine correlations
178 between the surface expression of CD73 and previously reported reservoir markers
179 and enrichment factors, including CD2, CD49d, PD-1, CD39, CD98, CTLA-4, CD20,
180 CD30 and CD32 in blood-derived CD4+ T cells from people living with HIV (PLWH).
181 CD4+ T cells were negatively-selected from fresh blood collected from six PLWH
182 on ART, and reservoir markers were measured by immunofluorescence staining
183 and flow cytometry. Notably, none of the previously identified reservoir markers
184 were enriched in the CD73+ CD4+ T cell compartment, and the frequency of PD-1
185 and CD39 expression was significantly reduced in CD73+ cells as compared to total
186 CD4+ cell populations (Figure S3 A and B). However, we also identified double-
187 positive cells co-expressing high levels of CD73 and CD49d, CD2, PD-1, or CD39,
188 respectively (Figure S3 C, red arrows), indicating that these markers are not
189 mutually exclusive *in vivo* in the setting of treated HIV infection. Expression levels
190 of CD98, CTLA-4, CD20, CD30 and CD32 were extremely low in both total CD4+ T
191 and CD73+ CD4+ T cells (Figure S3, B-D).

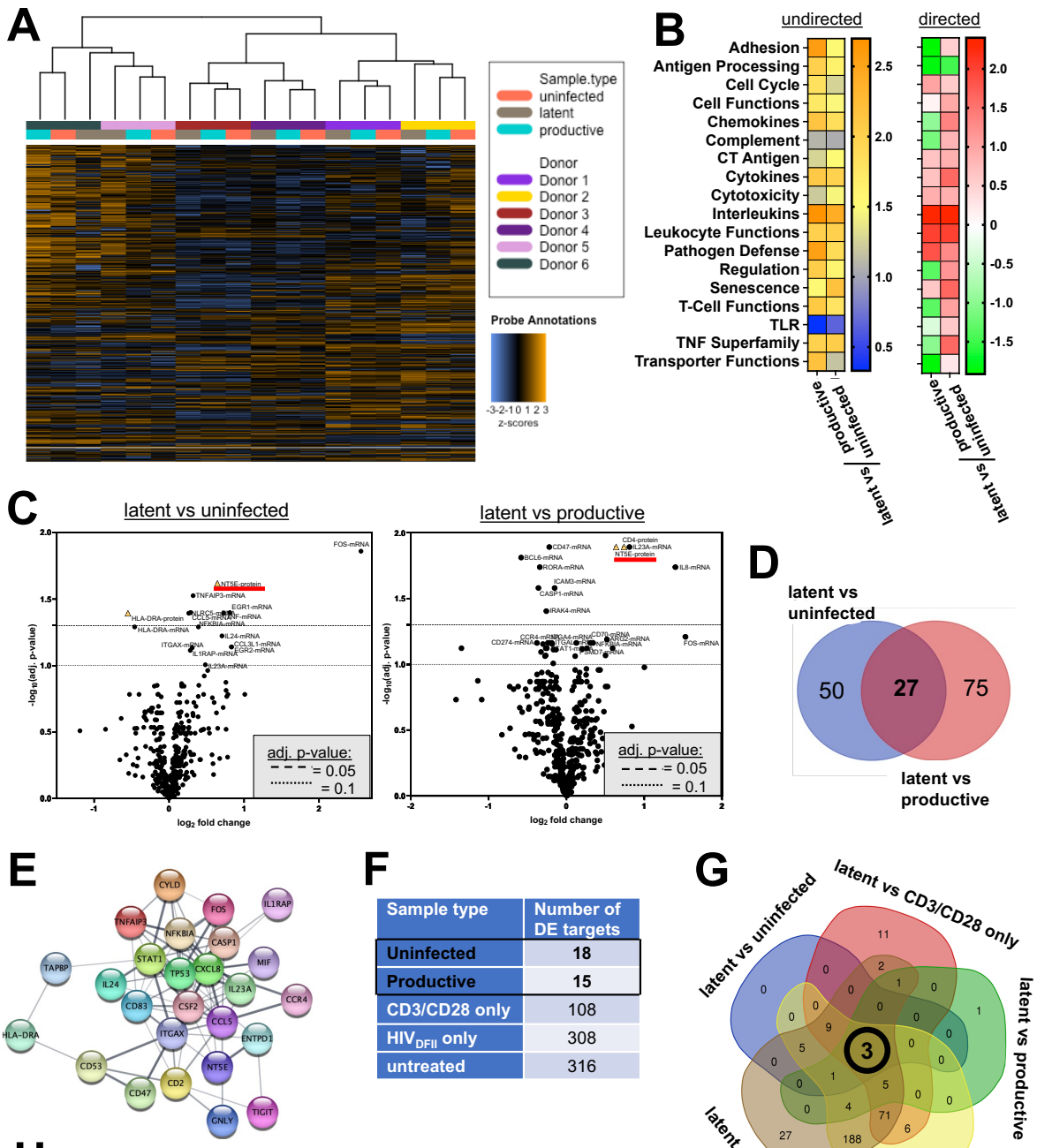

Sample type	Number of DE targets
Uninfected	18
Productive	15
CD3/CD28 only	108
HIV$_{DFII}$ only	308
untreated	316

192

193 **Figure 3: Latently-infected cells share signature features including distinct expression of IL8 mRNA,**
194 **CD39 mRNA and CD73 protein**. (A) Heatmap visualizing normalized gene expression data from unsupervised
195 clustering analysis of virus-exposed, sorted samples. Each row shows normalized counts of a single probe
196 (target) and each column represents an individual sample. Colored horizontal bars along the top identify
197 assigned sample attributes (donor or sample type, see color legend). Hierarchical clustering was used to
198 generate dendrograms. (B) Heatmaps showing undirected and directed global significance scores for signaling
199 pathways based on differential gene expression analysis. The level of significance is indicated from blue to
200 orange, the up- and down-regulation of pathways from red to green. (C) Volcano plots depict differential
201 mRNA (circle) and protein (triangle) target expression between latent vs uninfected and latent vs productively-
202 infected cells. Each data point represents one target. The $\log_2$ fold change is displayed on the x-axis and the -
203 $\log_{10}$ of the adjusted (adj.) p-value (using the Benjamini-Hochberg method) on the y-axis. Horizontal lines
204 indicate adj. p-value thresholds. The top 20 hits in each comparison are labeled. Hits were considered
205 significant at an adj. p-value cutoff < 0.1. NT5E (CD73) is underlined in red. (D) Venn diagram illustrating
206 overlapping hits from the DE analyses 'latent vs uninfected' and 'latent vs productive' using a p-value cutoff p
207 < 0.05. (E) A protein-protein interaction network of targets uniquely changed in latent cells was generated in
208 Cytoscape 3.8.2. The STRING database for Homo sapiens was applied with a confidence score of 0.4. Thickness
209 of lines between nodes depicts confidence score, with a thicker line representing a higher score. HLA-DRB3
210 was not recognized by the software and thus excluded from the interaction network. (F) Number of
211 differentially expressed genes from pairwise comparisons of latent cells to all other samples. Differential target
212 expression between samples was performed with a p-value cutoff at < 0.05. (G) Venn diagram displaying the
213 overlay of differential expression hits from comparisons of latently-infected cells with all other samples using
214 a p-value cutoff of p < 0.05. (H) Bar graphs depict the $\log_2$ fold change of the indicated targets between latent
215 cells and all other samples. Error bars show standard deviation (SD).

216 Based on unsupervised analyses including principal component analysis (PCA),
217 expression signatures were dominated by *in vitro* stimulation (Figure S4 A and B).
218 We therefore investigated T cell activation as a potential determinant of HIV
219 latency by examining the expression levels of established T cell surface markers
220 CD45, CD45RO, and CD4 (Figure S4 C), as well as panel-specific activation markers
221 (Figure S4 D and E). No significant associations were discovered between the
222 expression levels of these activation markers and latent infection, suggesting that
223 viral transcriptional fates are not dictated by cellular activation states.

224 **Hypoxia promotes CD73 expression and HIV latency in primary CD4+ T cells.**
225 To better understand the relevance of CD73 in the context of HIV infection and

226 particularly in the establishment of the latent reservoir, we next focused on the
227 regulation of CD73 expression[41,42]. Importantly, at least one hypoxia-response
228 element (HRE) has been previously identified in the CD73 promoter region[43]
229 allowing for direct binding of hypoxia-inducible factors (HIFs). In this context, HIF-
230 1 was demonstrated to control CD73 expression, with CD73 typically being
231 upregulated under hypoxic conditions[44]. We therefore hypothesized that our
232 discovery of CD73 upregulation in latent cells suggested that hypoxia may be the
233 underlying cause of both increased CD73 expression and HIV latency.

234 We first confirmed our NanoString data using *in vitro* infection with HIV_{DFII} followed
235 by immunofluorescence staining and flow cytometry, again observing a significant
236 enrichment of CD73+ cells among latently-infected cells (Figure 4A and B). We
237 then mimicked hypoxic conditions in our culture settings via administration of
238 dimethyloxalylglycine (DMOG), followed by infection with HIV_{DFII} and flow
239 cytometry (Figure 4C).

240 DMOG treatment substantially altered CD73 expression in CD4+ T cells and led to
241 a 2.5-fold increase of CD73+ cells compared to mock treatment (Figure 4D and E).
242 Similar levels of CD73 induction were observed in cells incubated at 1% oxygen,
243 indicating that DMOG treatment accurately recapitulates the CD73 phenotype in
244 CD4+ T cells (Figure S5A). Notably, while CD73 expression was generally increased
245 upon induction of hypoxic responses (compare Figure 4B and Figure S5B), we
246 observed a pronounced enrichment of CD73+ cells specifically in the latent
247 compartment with up to 60% of latent cells being CD73 positive (Figure S5B). This
248 was also reflected in CD73 expression per cell measured by mean fluorescence
249 intensities (MFIs), which showed an overall increased CD73 expression in latent
250 cells in both mock and DMOG-treated samples (Figure S5C). Latent infection
251 became significantly more abundant with a 33.6% increase upon DMOG treatment,
252 while the frequency of uninfected or productive cells did not change significantly
253 between culture conditions (Figure 4F and G).

254 Lastly, we examined whether CD73+ cells were enriched for latent virus (Figure 4H).
255 We measured a considerably higher rate of latently-infected cells in CD73+
256 compared to CD73- cells with an average 3-fold enrichment of latent infection
257 within the CD73+ T cell compartment (Figure 4I). Considering the average
258 frequency of CD73+ cells among CD4+ T cells (~10%, Figure 4E), these data
259 suggest that approximately 25% of the overall, peripheral CD4+ T cell HIV reservoir
260 may reside in CD73+ cells. Interestingly, the enrichment of latent cells in CD4+
261 CD73+ T cells did not significantly differ between mock- and DMOG-treated
262 samples (Figure 4I), indicating that CD73+ cells may possess specific features that
263 favor the establishment and/or maintenance of latent infection that are not further
264 modulated by the induction of hypoxic responses.

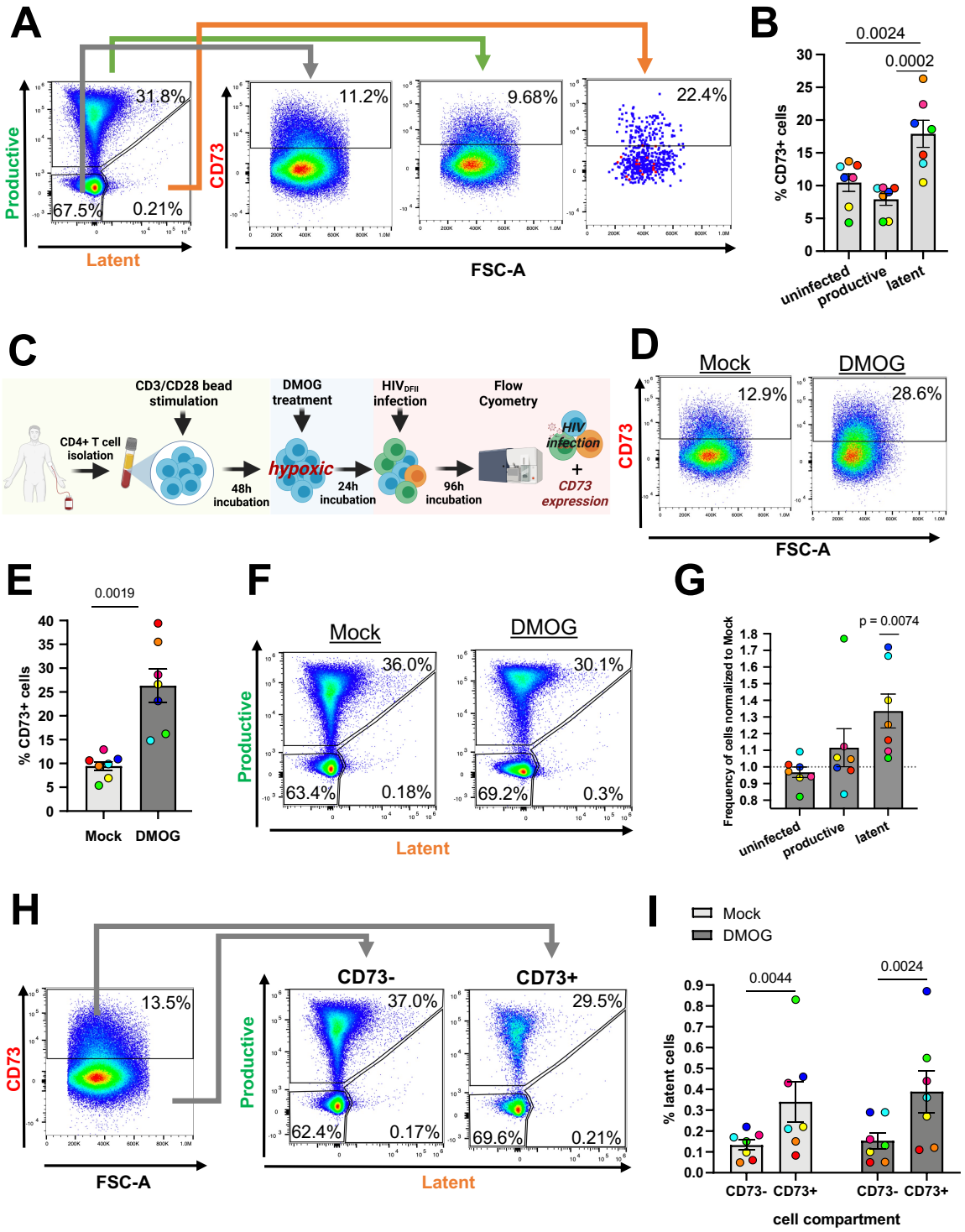

Figure 4: Hypoxic conditions increase the frequency of CD4+ CD73+ T cells and facilitate latent infection. (A) CD4+ T cells from healthy individuals were infected with HIV_{DFII} and analyzed by immunofluorescence staining and flow cytometry. Scatter plots show the gating strategy to analyze CD73 expression in HIV_{DFII}-infected cells from a single, representative donor. (B) Shown is the frequency of CD73+ cells in the respective HIV_{DFII}-infected cell population summarized from 7 donors. P-values displayed above

271 bars were generated by performing a one-way ANOVA with Tukey's multiple comparisons test. (C)
272 Experimental workflow for HIV_{DFII} infection under hypoxic conditions. (D) Representative flow plots of CD73
273 immunofluorescence staining in mock or DMOG treated CD4+ T cells and (E) average frequency of CD73+
274 CD4+ T cells across 7 donors. The p-value was generated by performing a two-tailed paired t-test. (F)
275 Representative flow plots, showing HIV_{DFII} infection profiles 4 days post HIV_{DFII} exposure upon mock or DMOG
276 treatment. (G) The frequency of DMOG-treated, HIV_{DFII}-infected cells was normalized to the respective mock
277 population within each donor to account for donor variability. P-values were generated by performing a two-
278 way ANOVA with Fisher's Least Significant Difference (LSD) test. (H) Gating strategy used to analyze HIV_{DFII}
279 infection profiles in the CD4+ CD73+/- T cell compartments. Data shown are from a single, mock-treated
280 donor and are representative for all seven donors. (I) The average frequency of latently-infected cells was
281 assessed in CD4+ CD73+/- T cells. Colored dots indicate individual donors. P-values were generated by
282 performing a two-way ANOVA with Fisher's LSD test. P-value threshold for significance was at $p < 0.05$. Error
283 bars show SEM.

284 **CD73+ cells exhibit distinct immunoregulation and tyrosine kinase signaling.**
285 The role of CD73 in the context of oncogenesis, tumor progression and survival is
286 well described[38]. However, relatively little is known about the relevance and
287 function of CD73 in human CD4+ T cells. We thus characterized the transcriptome
288 of blood-derived, primary CD73+ and CD73- CD4+ T cells by RNA sequencing. To
289 address this aim, CD73-/+ cells were isolated from primary CD4+ T cells by FACS,
290 revealing highly variable frequencies of CD73+ CD4+ T cells across donors, ranging
291 from ~3% to ~23% (Figure S6A and B). Sorted cells were then subjected to RNA
292 sequencing and DE analysis, accounting and adjusting for donor effects (Figure
293 S6C and D). CD73- and CD73+ CD4+ T cells exhibited distinct transcriptional
294 profiles and a clear clustering of the sorted populations (Figure 5A). Expectedly, the
295 CD73 (*NT5E*) exhibited highly significant divergence in expression levels between
296 groups (Figure 5B). An additional 145 genes were differentially expressed, with 111
297 upregulated and 34 downregulated genes in CD73+ cells (Figure 5B). *CR1,*
298 *ADAM23, ABCB1 and AUTS2* were among the top genes upregulated in CD73+
299 cells (Figure 5B, yellow dots). *CLEC17A* exhibited the highest fold change (> 5-fold),
300 followed by *CD73, LINC02397* and *MACROD2* (> 4-fold) (Figure 5B, red dots).
301 Multiple genes were markedly downregulated in CD73+ cells; however, only two

302 of them reached the highest level of statistical significance (adjusted $p < 0.01$):
303 *FCER1A* and *NPR3*. A gene set enrichment analysis yielded a multitude of
304 significantly modulated pathways differentiating CD73+ and CD73- cells including
305 'immune responses', 'complement activation' and 'receptor-mediated signaling
306 cascades' (Figure 5C), indicating diverging immunoregulatory programs. In
307 addition, 'positive regulation of angiogenesis', 'regulation of apoptotic processes'
308 and 'tyrosine kinase signaling cascades' were among the 40 most significantly
309 modulated pathways.

310 Next, all differentially expressed genes were uploaded into Cytoscape and the
311 resulting protein-protein interaction network was then overlaid with $\log_2$ fold
312 changes and adjusted p-values of each gene, visualizing directionality and
313 significance of interacting hits (Figure 5D). The analysis revealed five distinct
314 interaction networks, with one network containing the majority of hits. This
315 approach revealed biological programs associated with the CD73+ CD4+ T cell
316 compartment. Within this network, a tight cluster (I) of cell surface receptors was
317 apparent (*CD22, CD79A, CR1, CR2, KIT, FCER1A, CD34*), accompanied by several
318 signaling factors (*LYN, BLNK, BLK, BTK, PIK3AP1, TCL1A)* and transcription factors
319 (*IRF8, EBF1, PAX5*). Another cluster (II) comprised downregulation of cell surface
320 proteins *CXCR3*, *CCR4* and *PTGDR2*. Importantly, the network also contained two
321 significantly downregulated genes, transcription factor *GATA2*, and DNA
322 topoisomerase *TOP2A*, which are known to support active HIV transcription and
323 replication[45,46].

324 **CD73+ CD4+ T cells harbor an inducible HIV reservoir.** The intactness of
325 integrated proviruses and the inducibility of viral gene expression are key attributes
326 of the latent HIV reservoir. We therefore sought to investigate the capacity of
327 CD73+ T cells to harbor reactivatable latent virus. To this end, we adapted a
328 primary *in vitro* HIV infection model[47] and infected FACS-sorted CD73- and CD73+
329 CD4+ T cells with the reporter virus HIV_{Luc} (Figure 5E). After a resting period of 5

330 days, we stimulated cells with αCD3/αCD28 beads and observed a pronounced
331 increase of viral transcription in both CD73- and CD73+ CD4+ T cells as compared
332 to unstimulated cells, reflected by a 10-fold and 14-fold increase in LTR-driven
333 luciferase activity, respectively (Figure 5F). Induction of viral transcriptional activity
334 was significantly higher in stimulated CD73+ T cells as compared to CD73- T cells.
335 These results demonstrate that the CD73+ CD4+ T cell compartment can harbor
336 an inducible latent reservoir *in vitro*, indicating the potential of this compartment
337 to contribute to spreading infection in people PLWH upon treatment cessation.

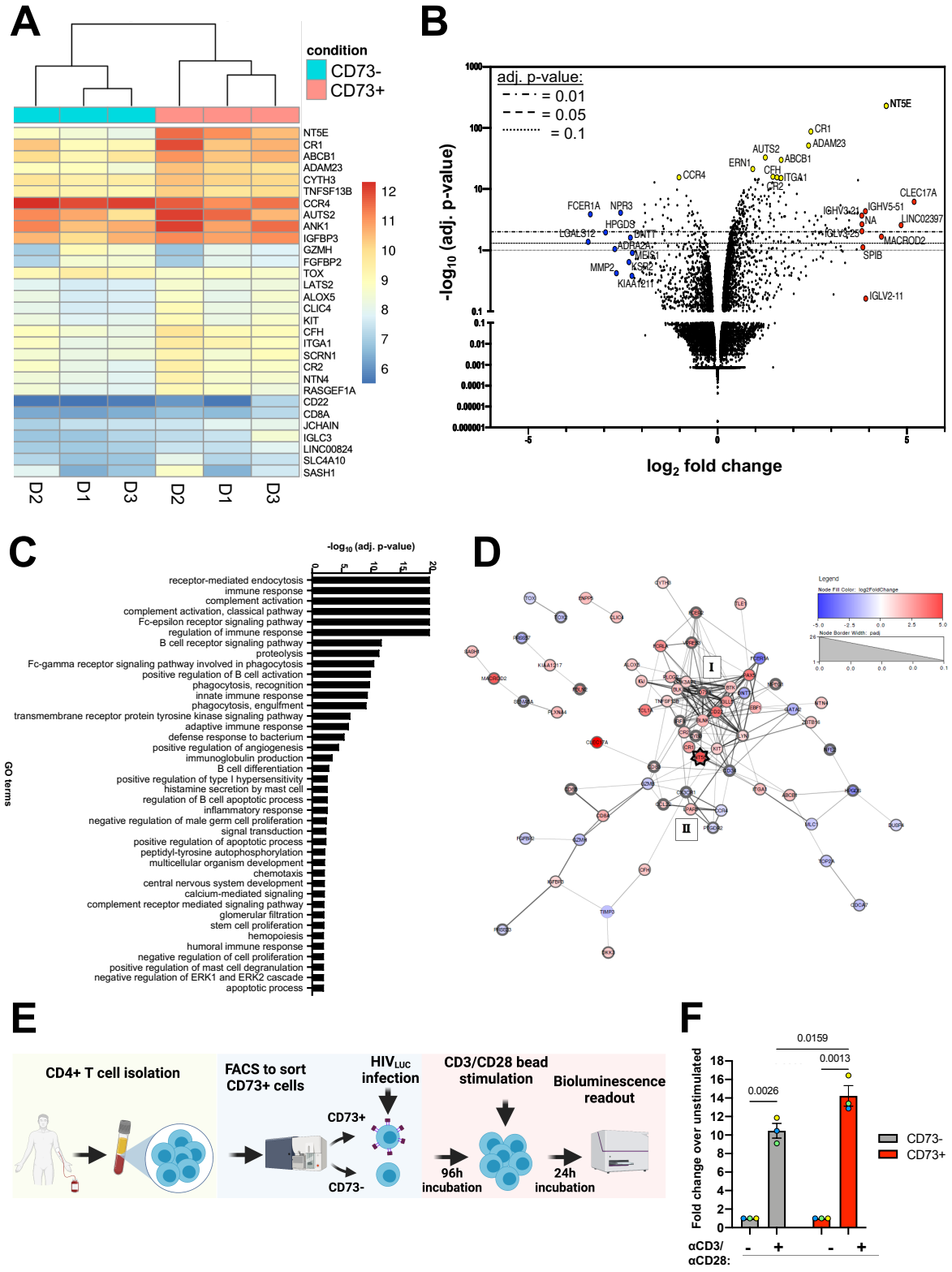

Figure 5: CD73+ cells exhibit distinct immunoregulatory features and support HIV reactivation. (A) Clustering heatmap visualizing the expression profile of the top 30 differentially-expressed genes sorted by their adjusted p-value. Data were adjusted for donor effects. (B) Global transcriptional changes between CD73-

342 and CD73+ cells are visualized in the volcano plot. Each data point represents a single gene. The log_2 fold
343 change of the normalized mean hit counts of each gene are plotted against $-log_{10}$ of its adj. p-value (using the
344 Benjamini-Hochberg method). Horizontal lines indicate adj. p-value thresholds. The top 10 most significantly
345 changed (yellow), most upregulated (red) and most downregulated (blue) genes are highlighted. (C)
346 Differentially expressed genes were grouped by their gene ontology (GO) and the enrichment of GO terms
347 was tested using Fisher exact tests. The top 40 GO terms with an adj. p-value < 0.05 are displayed. (D) The
348 protein-protein interaction network of genes differentially expressed between CD73- and CD73+ CD4+ T cells
349 was generated in Cytoscape as described previously. 33/145 hits were not recognized by the STRING database
350 and thus excluded from the interaction network. Among the remaining 112 genes, 43 genes did not have an
351 interaction partner and are not displayed. Log_2 fold changes of genes are indicated by node pseudo color and
352 the adj. p-value by node border width. *CD73* (*NT5E*) is highlighted by a star shape. Protein clusters of interest
353 are labeled. (E) The schematic represents the experimental workflow to test reactivation of integrated provirus
354 in sorted CD73- and CD73+ CD4+ T cells. (F) Bars display the average fold change over unstimulated cells
355 from three donors. Colored dots indicate individual donors. P-values above bars were generated by performing
356 a two-way ANOVA with Fisher's LSD. A p-value at $p < 0.05$ was considered significant. Error bars show SEM.

357 **Blocking the adenosine receptor A2AR or CD73 promotes HIV latency**
358 **reversal**. Bearing in mind the enzymatic function of CD73, we hypothesized that
359 extracellular adenosine produced by CD73 could be mechanistically involved in the
360 establishment and/or maintenance of HIV latency. To test this, we investigated the
361 adenosine signaling cascades downstream of CD73 in the well-established J-Lat
362 cell line models of latency[48,49], exploring how modulation of adenosine receptors
363 by small molecule drugs affects HIV transcriptional activity.

364 First, CD73 surface expression was measured in J-Lat clones, 5A8, 6.3, 11.1, and A72
365 as well as in the parental JurkatE6 cell line (Figure 6A). We found that between 10-
366 20% of JurkatE6, J-Lat 6.3, 11.1, and A72 cells expressed CD73 on the surface,
367 whereas about 80% of J-Lat 5A8 cells were CD73 positive. In the next experiment
368 we sought to test whether an inhibition of adenosine signaling will impact HIV
369 transcription in J-Lat cells. To that aim, J-Lat 5A8 cells were pretreated with the
370 adenosine receptor antagonist SCH-58261 (SCH), followed by viral reactivation
371 with PMA/I, a strong mitogen and latency reversing agent. Notably, pretreatment
372 with SCH significantly promoted latency reversal and resulted in an evident dose
373 response with a 2-fold increase in the frequency of GFP+ cells at the highest dose

374 (Figure 6B). At the same time, SCH pretreatment did not compromise cell viability
375 at any dose compared to cells treated with PMA/I only (Figure 6B).

376 Finally, we sought to determine if downregulation of CD73 itself affects HIV
377 transcription and latency reversal. To pursue this objective, we performed CD73
378 knockdown (KD) via CRISPR interference (CRISPRi) in the A72 J-Lat clone. We first
379 introduced the CRISPRi effector protein dCas9-KRAB by lentiviral transduction,
380 generating the cell line J-Lat A72 CRISPRi. We then utilized another lentiviral vector
381 to express single guide RNAs (sgRNAs) targeting CD73 or a non-targeting (NT)
382 negative control, respectively. We tested KD efficiency by immunofluorescence
383 staining of surface CD73, finding a significant downregulation of CD73 compared
384 to non-targeting controls (Figure 6C). CD73 KD resulted in significantly lower GFP
385 expression levels in both stimulated and non-stimulated conditions (Figure 6C),
386 indicating that CD73 exerts direct effects on HIV transcription and latency.

387 **A comprehensive model of CD73-dependent latency.** Based on our data
388 obtained in *in vitro* infection models, we devised a model that incorporates
389 hypoxia, CD73, and adenosine signaling, linking these factors with HIV
390 transcriptional regulation and persistence. Our model predicts that the hypoxia-
391 CD73-adenosine (HCA) axis plays a vital role with CD73 as a central player in the
392 maintenance of latent HIV infection (Figure 6D): As is known, HIV preferentially
393 persists in lymphatic tissues[50], which exhibit low oxygen levels and thus high levels
394 of active HIFs. We surmise that the resulting upregulation of CD73 expression leads
395 to adenosine-rich, immunosuppressive microenvironments, which promote the
396 establishment and maintenance of latent reservoirs. Accumulation of extracellular
397 adenosine thereby creates optimal conditions for HIV persistence by suppressing
398 HIV host dependency factors through autocrine signaling cascades, while
399 impairing effective host immune responses through paracrine signaling
400 mechanisms. Therefore, viral transcription is repressed, and immune escape of HIV-

infected cells is facilitated, altogether promoting viral quiescence and survival of the latent reservoir.

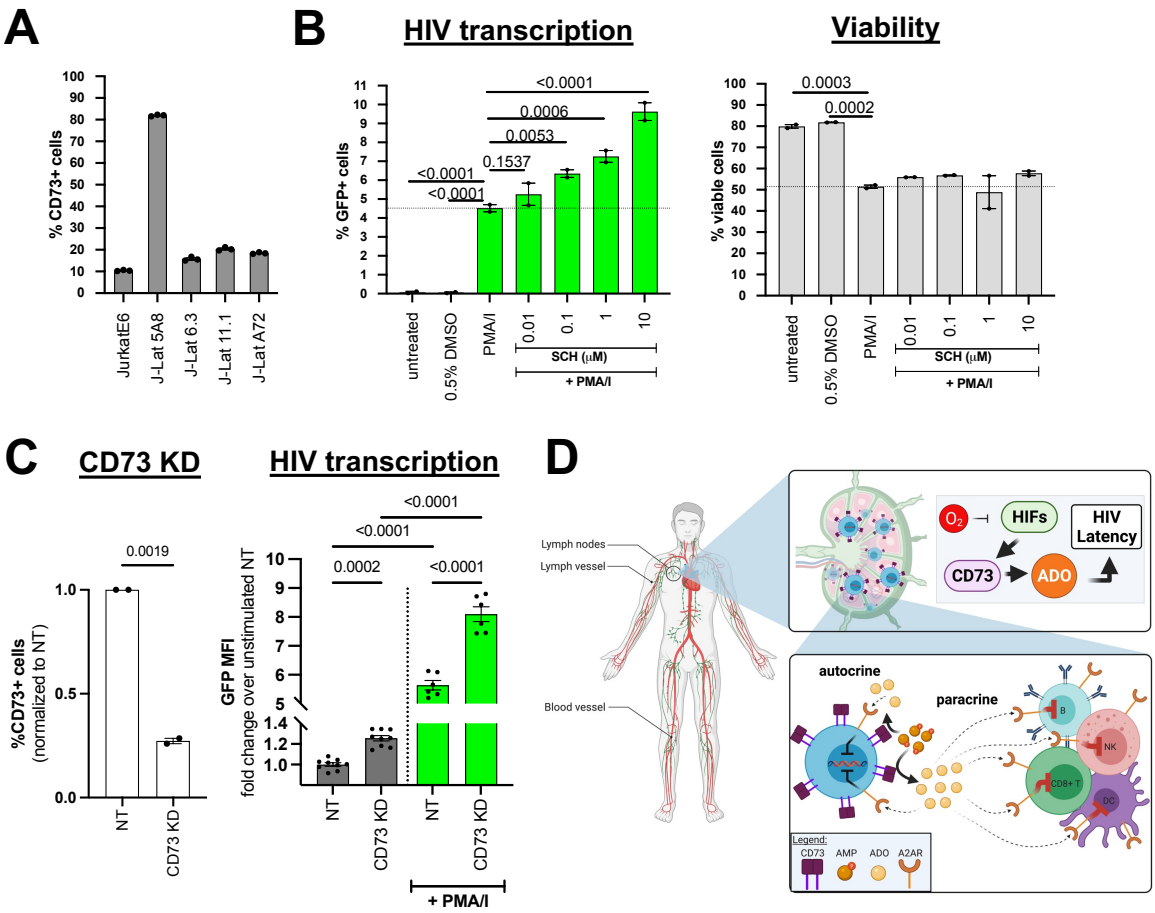

Figure 6: Blockade of CD73 and adenosine receptor A2AR facilitates HIV latency reversal. (A) Average frequency of live, single CD73+ cells in the different T cell lines measured via flow cytometry. (B) J-Lat 5A8 cells were treated with A2AR antagonist SCH-58261 (SCH) at indicated, increasing doses for 1h, followed by treatment with PMA/I. PMA/I treatment alone served as positive control, 0.5% DMSO treatment as mock control. Cell viability based on FSC-A and SSC-A and GFP expression as a reporter of HIV transcriptional activity was assessed 7h post treatment using flow cytometry. Samples were measured in duplicates. P-values were generated by performing a one-way ANOVA with Fisher's LSD. $p < 0.05$ was considered significant. Data represent the mean and error bars the SEM. (C) J-Lat A72 cells were transduced with lentiviral vectors containing dCas9-KRAB sgRNAs targeting CD73 or a non-targeting control (NT). CD73 KD was assessed via immunofluorescence staining of CD73 as measured by flow cytometry. Data were normalized to NT. Reactivation of viral transcription reflected by GFP expression was assessed by flow cytometry of A72 KD cells in presence and absence of PMA/I. Significance was determined by one-way ANOVA, comparing samples with NT. (D) HCA-model of HIV persistence. Under long-term ART, HIV persists in vivo preferentially in anatomical sanctuary sites like lymph nodes. Oxygen levels are known to be significantly lower in lymphoid tissues (0.5-

418 4.5%) compared to the periphery (about 13%). Low oxygen supply or hypoxia lead to stabilization of hypoxia
419 inducible factors (HIFs) which control the expression of CD73. Upregulation of CD73 leads to the accumulation
420 of adenosine (ADO) in the extracellular space. These factors favor the establishment of viral reservoirs and
421 promote HIV persistence, silencing the provirus through autocrine signaling and inhibiting host antiviral
422 immune responses by paracrine signaling mechanisms. T cells are shown in blue, CD73 in purple.

423 **Detection of HIV markers and CD73 *in vivo* in tissues from ART-suppressed**
424 **HIV-infected individuals.** To evaluate the clinical relevance of our findings and to
425 test the HCA model *in vivo*, we applied a comprehensive tissue imaging pipeline
426 that enables simultaneous detection of integrated HIV-DNA, viral mRNA, and HIV
427 protein, as well as lineage markers, followed by quantitative image analyses[51–53].
428 We concomitantly detected CD73 expression and HIV markers in lymph node
429 tissues (peripheral and inguinal lymph nodes) obtained from HIV-infected
430 individuals on suppressive ART (ART suppr.), as well as in viremic untreated
431 individuals, and uninfected controls (Figure 7A). CD3 staining was used as a lineage
432 marker for T cells and DAPI was included as a counter staining of nuclear DNA.
433 CD73 signals were found across all samples, while HIV detection expectedly
434 differed greatly between ART-suppressed and viremic individuals and was absent
435 in uninfected control samples (Figure 7A and B). Quantification of the viral reservoir
436 in viremic individuals indicated that at least 40% of CD3+ cells harbored integrated
437 DNA and most of these cells expressed viral RNA and HIV-p24 (Figure 7B, viremic).
438 In contrast, in ART-suppressed individuals, 0.017% of CD3+ cells contained viral
439 DNA, half of which expressed viral RNA and 10% of which expressed viral proteins
440 (Figure 7B, ART-suppr.).

441 **CD73 expression correlates with HIV persistence in lymph nodes from ART-**
442 **suppressed individuals.** Next, we determined the association between HIV
443 infection and CD73 expression, specifically in the CD3+/CD3- cell compartment
444 (Figure 7C). CD73 expression levels in CD3+ cells were significantly higher in ART-
445 suppressed samples than in uninfected samples. In addition, HIV DNA+ CD3+ cells
446 in ART-suppressed individuals exhibited a significant, 1.6-fold higher CD73

447 expression compared to the overall CD3+ population. This difference in CD73
448 expression levels was not observed in viremic individuals and suggested that CD73
449 expression may offer a survival advantage for HIV-infected cells in the setting of
450 ART. We further hypothesized that viral reservoirs would not only reside in
451 individual CD73+ cells, but rather in CD73-rich, HIV persistence-promoting
452 microenvironments, due to local hypoxia and paracrine adenosine signaling
453 effects. To explore this hypothesis, we performed imaging analysis by measuring
454 the expression of CD73 in CD3+/HIV-DNA+ cells as well as neighboring uninfected
455 cells surrounding viral reservoirs (Figure 7D and Figure S7). Zero represents foci of
456 viral infection, and increasing or decreasing distances correspond to neighboring
457 uninfected cells (Figure 7D, up to 80 μm). Most localized expression of CD73 was
458 observed in and around viral reservoirs (CD3+HIV-DNA) in ART-suppressed
459 individuals. In addition, we observed that CD3+ cells that were negative for HIV-
460 DNA but HIV-p24 positive (HIV-DNA^{-}/p24^{+}), perhaps due to the uptake of viral
461 particles, also had increased levels of CD73. In contrast, evenly-distributed
462 expression of CD73 was observed in uninfected and viremic lymph node tissues,
463 confirming that the spatial association between CD73 expression and viral
464 reservoirs is specific to ART-suppressed HIV infection (Figure 7D, black and green
465 lines, respectively). Our data indicate that HIV DNA+ CD3+ cells in lymph nodes
466 from ART-suppressed individuals reside in areas with generally high CD73
467 expression, reinforcing that CD73 via adenosine production contributes to HIV
468 persistence (Figure 7D).

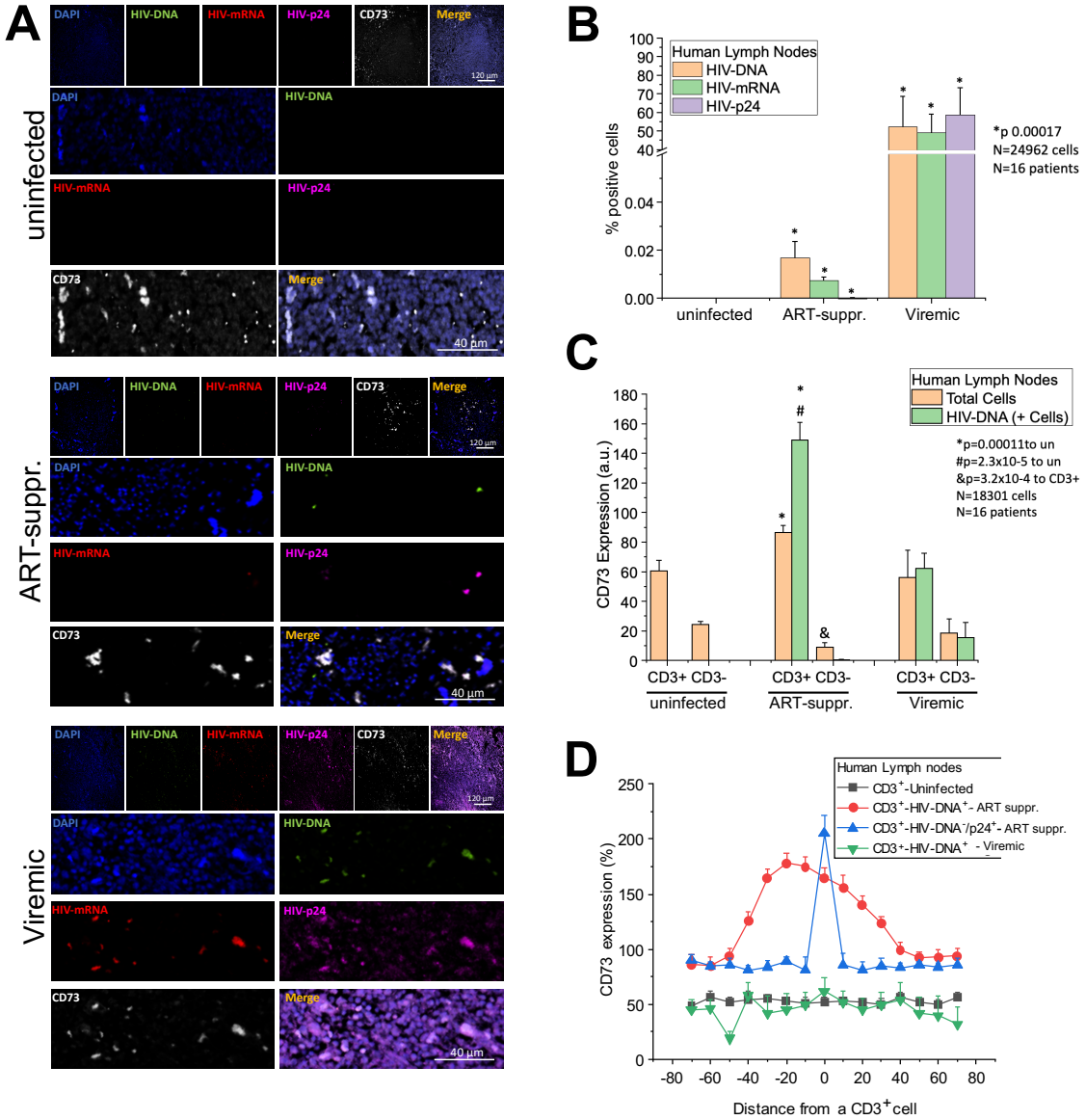

Figure 7: *In situ* imaging of lymph nodes from PLWH reveals associations between CD73 protein expression and HIV DNA specifically in ART-suppressed individuals. (A) Panels show representative confocal microscopy images for CD73 and HIV marker staining of lymph node tissue obtained from uninfected, ART-suppressed (suppr.), and viremic individuals. (B) Automated image analysis of tissue sections stained for HIV DNA, mRNA and p24 protein in uninfected (n = 5), ART-suppressed (n = 6), and viremic individuals (n = 5). Bar graphs show the average percentage of cells that exhibit a positive signal for the respective target. (C) Quantitative CD73 expression analysis in tissue samples from uninfected (n = 5), ART-suppressed (n = 6) and viremic individuals (n = 5). Identification of the T cell compartment (CD3+ cells) and detection of HIV reservoir cells (HIV-DNA+) was followed by quantification of CD73 signals in the indicated 4 cellular subsets (CD3+ HIV-DNA-, CD3+ HIV-DNA+, CD3- HIV-DNA-, CD3 HIV-DNA+). ANOVA was used to compare groups. Relevant statistics are shown in bar graphs. (D) Quantification of CD73 expression and distribution in and around viral

481 reservoirs in μM. Lineplot analysis was performed as described in the Methods section and the schematic
482 shown in Figure S7. 40-98 3D reconstructed images were analyzed per condition from 16 independent
483 participant samples. CD73 intensity values were normalized to mean intensities in CD3+ HIV-DNA-/p24+-ART
484 suppr. samples.

485

DISCUSSION

The latent HIV reservoir is considered to be the main obstacle to achieving viral eradication or indefinite disease remission in the absence of ART. It is generally believed that integrated provirus persists in specific cellular compartments and tissue sanctuaries which enable both long-term survival and spontaneous reactivation of viral replication even after decades of successful ART. The exact identity of the HIV reservoir however remains elusive. The goal of this study was to thoroughly characterize primary HIV latently-infected cells using comprehensive and complementary systems approaches. Our work focused on CD4+ T cells, the major target of HIV infection and an important potential source of viral rebound upon ART interruption.

The core finding of this work was the identification of elevated cell-surface expression of CD73 as a signature characteristic of HIV latently-infected CD4+ T cells – an observation that, to the best of our knowledge, has not been described before. Using different *in vitro* models of HIV latency, we found indications that CD73 is not merely a passive marker of reservoir cells, and regulation of CD73 expression as well as its enzymatic function is mechanistically linked to HIV persistence.

Our NanoString analyses also revealed significant changes in the expression of CD39 and IL8 within the latent compartment, which are mechanistically connected to CD73. In particular, the two ectonucleotidases CD39 and CD73 and their orchestrated functionality in purinergic signaling are well described in the literature[38–40]. In addition, IL8 expression has been shown to be stimulated by adenosine signaling, and is thus directly linked to the enzymatic function of CD73[37]. The distinctive expression of these three factors in latent cells suggests that CD73 and the adenosinergic pathway play a pivotal role in HIV latency and the establishment and/or maintenance of viral reservoirs.

513 Our initial *in vitro* infection model using HIV_{DFII} focused on a rather narrow time
514 window of HIV latency, recapitulating the establishment and early persistence of
515 viral reservoirs within a few days after infection. In the setting of HIV infection *in*
516 *vivo*, HIV persists even after decades of fully suppressive ART. Linking the two
517 observations, our *in situ* imaging of lymph node tissues demonstrated, for the first
518 time, that a significant association between CD73 expression in T cells and HIV-
519 DNA specifically in ART-suppressed individuals is maintained over extended
520 periods of time. No spatial associations between CD73 and HIV markers were
521 observed in tissues from viremic, untreated individuals. We surmise that in the
522 absence of treatment, when HIV is not subject to pharmacologic selection pressure,
523 active viral replication overrides CD73 effects and leads to rapid turnover of
524 infected cells. In the setting of long-term ART, HIV-infected cells are subject to
525 immune selection pressure, leading to an enrichment in CD73+ infected cells due
526 to their immunosuppressive nature and their increased likelihood of harboring
527 transcriptionally inactive virus. This hypothesis is further reinforced by our
528 transcriptomic profiling of blood-derived CD73+ and CD73- CD4+ T cell subsets
529 which revealed a spectrum of biological programs in the CD73 compartment that
530 are expected to promote viral quiescence, immune evasion, and cell survivorship.

531 A key finding of our study is that CD73 is significantly upregulated under hypoxic
532 conditions in the CD4+ T cell compartment. This result is important for two reasons:
533 1) Oxygen tension levels are highly variable throughout the body, ranging from
534 110 mmHg in well oxygenated lung alveoli[54], down to 55 – 60 mmHg[55] in the
535 gastrointestinal tract, and 3 – 35 mmHg in lymphoid organs[56,57]. As a consequence,
536 immune cells including CD4+ T cells encounter and operate at varying oxygen
537 concentrations as they traffic through the body[57]. Lymphoid organs in particular
538 represent crucial viral sanctuaries and as these are characterized by low oxygen
539 levels, our data suggest a causal link between hypoxia, CD73 expression, and HIV
540 persistence. 2) Hitherto, the role of oxygen levels and hypoxia in HIV infection

541 remained intangible and somewhat obscure. In 2009 Charles et al.[58] reported
542 decreased HIV-1 RNA levels at 3% oxygen, while S. Deshmane and colleagues
543 showed increased HIV transcription mediated by the interaction between HIV
544 accessory protein Vpr and HIF-1α[59,60]. Moreover, HIV-1 replication was shown to
545 be promoted by HIF-1α which in turn was stabilized by reactive oxygen species[61].
546 Very recently it was demonstrated that hypoxia can promote HIV latency with HIF-
547 2α as a direct inhibitor of viral transcription[62]. Our data now provide new insights
548 into the connection between HIV latency and hypoxia, with CD73 emerging as key
549 mediator bridging hypoxia and viral transcription.

550 As outlined above, our data suggest mechanistic involvement of CD73 in HIV
551 persistence via its enzymatic function in the adenosine signaling cascade.
552 Adenosine signaling leads to a suppression of cellular transcription factors that are
553 critical for active viral transcription[63,64] and may create an ideal immunological
554 niche for infected cells to evade host immune clearance due to an adenosine-
555 mediated immunosuppressive microenvironment. Pharmacological blockade of
556 A2AR in our latency model facilitated HIV latency reversal without impairing cell
557 viability. Thus, our data demonstrate the potential of targeting the adenosinergic
558 system as a therapeutic approach in the context of HIV infection and provides first
559 evidence that the enzymatic activity of CD73 is directly involved in HIV persistence.
560 We would like to point out that hypoxia can regulate the expression of numerous
561 genes[65], including, but not limited to CD39, the adenosine receptor ADORA2B, the
562 equilibrium nucleoside transporter ENT-1 and adenosine kinases (ADK)[66], all of
563 which could promote adenosine signaling independent of, or in concert with CD73.
564 Additional studies will therefore be necessary to determine how these diverse
565 factors link hypoxia-mediated signaling to HIV persistence.

566 It is important to note that in recent years increasing circumstantial evidence has
567 been gathered, independently suggesting a critical role for either hypoxia[58–62],
568 CD73 expression[67–69] or adenosine signaling[70–74] in HIV infection. Our findings

569 reported here are complemented and validated by a recent translational study by
570 Seddiki *et al.* demonstrating that HIV-infected CD73+ memory CD4+ T cells
571 contribute significantly to the very long-lived HIV proviral DNA reservoir in treated
572 subjects[75]. Our data now reveal a direct, causal connection that links the hypoxic
573 regulation and adenosine-producing enzymatic activity of CD73 to the
574 establishment and persistence of viral reservoirs.

575 Finally, the CD73-adenosine axis has received a great deal of attention in the
576 context of cancer biology[76–78] and the adenosinergic system has emerged as a
577 promising new drug target in oncology[37,38,79–84]. Our data suggest that, like solid
578 tumor cells, latent HIV reservoirs hijack the CD73-adenosine axis to subvert innate
579 and adaptive immune responses, enhancing the survivorship of the infected cell as
580 a persistence mechanism during ART. Therefore, CD73- and adenosine-focused
581 anti-cancer therapeutics should be actively explored as foundations of novel HIV
582 cure approaches and host-directed therapies.

583 **Limitations of the study.** There are limitations to both our in vivo models and our
584 in vivo profiling work that should be considered. Firstly, our in vitro HIV latency
585 models are short-term infection models, which were mainly geared at identifying
586 host factors associated with the establishment of viral transcriptional latency in
587 newly-infected cells. These models do not capture the critical aspects of
588 immunological selection that occur in vivo over the course of years or even
589 decades of suppressive ART in PLWH; long-term selection pressures in vivo may
590 result in enrichment of host factors on the surface of latently-infected cells that do
591 not appear in our in vitro profiling experiments. In regards to our in vivo profiling
592 of lymphoid tissues, analyses of a much larger collection of tissue samples (from a
593 broader array of anatomic sites associated with HIV persistence) will be required
594 to fully appreciate the association between CD73 expression and the HIV reservoir.
595 Moreover, our studies here have not considered HIV persistence outside of the
596 lymphoid compartment; as there is evidence that myeloid lineage cells (e.g.

597 monocyte-derived macrophages) harbor HIV, the relevance of adenosine signaling
598 to HIV infection should be evaluated in these cell types as well. Lastly, although
599 our in vitro experiments provide mechanistic connections between adenosine
600 signaling and HIV persistence, much additional work remains to be done to
601 decipher the relationship between adenosine signaling, HIV latency, and antiviral
602 immunity in vivo. These future studies will be critical in guiding the development
603 of novel HIV cure strategies targeting the adenosine pathway.

604

605 **MATERIALS AND METHODS**

606 **Construction of next generation HIV_{DFII} reporter plasmid.** The 1st generation
607 dual reporter virus construct R7GEmC[26] (kindly provided by Dr. Eric Verdin) was
608 adapted by ligation-based molecular cloning. Briefly, R7GEmC was linearized by
609 enzymatic digest using FseI and AscI (New England Biolabs, Cat. #R0588S and Cat.
610 #R0558S) in order to excise the mCherry open reading frame. Then, mKO2 was PCR
611 amplified from the template mKO2-N1 (Addgene, Cat. #4625) using primers
612 containing matching restriction sites. Subsequently, the lentiviral vector was
613 dephosphorylated using Quick CIP (New England Biolabs, Cat. #M0525S), purified
614 and subjected to ligation with the digested and gel-purified PCR product utilizing
615 T4 DNA ligase (New England Biolabs, Cat. # M0202S).

616 **Plasmid amplification and preparation.** Circularized plasmid DNA was
617 transformed by heat-shock in chemically competent Stbl-3 E. coli (ThermoFisher
618 Scientific, Cat. #C737303) for subsequent antibiotics selection and Sanger
619 sequencing (Elim Biopharm) of positive clones.

620 Transformed Stbl-3 cells were grown in 2-5 ml of lysogeny broth with 0.1 mg/ml
621 Ampicillin (LB Amp) for 16-24h or 4-8 hours prior to inoculation of large-volume
622 flask with 100-300 ml LB Amp for overnight growth. 16 hours later, cells were
623 pelleted by centrifugation for 15 min at >3000 g and subjected to plasmid
624 preparation using the NucleoSpin Plasmid, Mini kit for plasmid DNA (Macherey-
625 Nagel, Cat. # 740588) or Plasmid Plus Maxi Kits (QIAGEN, Cat. #12963) following
626 the manufacturer's protocol. Concentrations of isolated plasmid DNA was
627 spectrophotometrically determined using a NanoDrop 1000 (ThermoFisher,
628 Scientific) and DNA aliquots were stored at 4°C.

629 **Cell lines and cell culture.** HEK293T were obtained from ATCC and were cultured
630 in DMEM (ThermoFisher, Scientific, Cat. # 11965-118) supplemented with 10% FBS
631 (Corning, Inc., Cat. #35-010-CV) and 10% Penicillin/1% Streptomycin (Fisher
632 Scientific, Cat. #11548876) (DMEM complete = DMEM+/+) at 37°C, 5% CO_2 unless

633 stated otherwise. J-Lat 5A8 cells were kindly provided by Warner C. Greene
634 (Gladstone Institutes) and J-Lat A72 cells were obtained from the NIH HIV Reagent
635 Program (Cat. # ARP-9856). All other J-Lat clones were a gift from Eric Verdin (Buck
636 Institute). Jurkat E6-1 cells were obtained from ATCC. All suspension cells were
637 cultured in RPMI 1640 (ThermoFisher, Scientific, Cat. #11875-119) supplemented
638 with 10% FBS and 10% Penicillin/1% Streptomycin (RPMI complete = RPMI+/+) at
639 37°C, 5% CO_2 unless stated otherwise.

640 **Virus production.** HIV-1 viruses were generated by transfection of proviral DNA
641 into HEK293T cells via polyethylenimine (PEI, Polysciences, Cat. #23966)
642 transfection protocol. Env-pseudotyped HIV_{DFII} stocks were produced by co-
643 transfecting plasmids encoding HIV_{DFII} and a plasmid encoding HIV-1 dual-tropic
644 envelope (pSVIII-92HT593.1, NIH HIV Reagent Program, Cat. #3077) at a ratio of
645 3:1 into HEK293T cells at 50-60% confluency grown in 175 cm^2 culture flasks. Each
646 flask was transfected with a total amount of 30 µg DNA. The transfection mix was
647 prepared in 2 ml Opti-MEM (ThermoFisher Scientific, Cat. #31985062) as follows:
648 DNA plasmids were diluted in Opti-MEM first, then PEI was added at a ratio of 3:1
649 PEI:DNA (90 µg PEI). The transfection mix was vortexed for 15 sec and incubated
650 for 15 min at RT. Culture medium was replaced with 20 ml fresh DMEM + 10% FBS
651 <u>without P/S</u>, and 2 ml transfection mix was added to each flask. 16h post
652 transfection, P/S-free medium was replaced with standard culture medium
653 (DMEM+/+), and cells were incubated for another 24h at 37°C, 5% CO_2. For
654 replication competent HIV NL4-3 Luciferase (a kind gift from Dr. Warner Greene),
655 lentiviral vectors were introduced by Fugene HD transfection (Promega, Cat.
656 #E2311) according to the manufacturer protocols. Cell supernatants were collected
657 48h post transfection, centrifuged at 4°C for 10 min at 4000 rpm (~ 3390 x g) and
658 subsequently filtered using 0.22 µm membrane vacuum filter units (MilliporeSigma,
659 Cat. #SCGP00525) to remove cell debris. Virus preparations were concentrated by
660 ultracentrifugation at 20,000 rpm (~ 50,000 x g) for 2h at 4°C and resuspended in

661 complete media for subsequent storage at -80°C. Virus concentration was
662 estimated by p24 titration (HIV-1 alliance p24 ELISA kit, PerkinElmer, Cat.
663 #NEK050001KT).

664 **Generation of CRISPRi cell lines.** Stable, knockdown cell lines were generated by
665 lentiviral transduction of dCas9-KRAB, as well as single guide RNAs (sgRNAs). We
666 first generated a CRISPRi cell line by transducing J-Lat A72 with the vector lenti-
667 EF1a-dCas9-KRAB-Puro (Addgene #99372, a gift from Kristen Brennand). After
668 selecting with puromycin-containing media (1 µg/ml) for at least one week, J-Lat
669 A72 CRISPRi were tested by qPCR for transgene expression using Cas9-specific
670 primers. Then, J-Lat A72 CRISPRi cells were transduced with the lentiviral vector
671 pLKO5.sgRNA.EFS.tRFP (Addgene #57823, a gift from Benjamin Ebert), containing
672 target-specific sgRNAs (J-Lat A72 CRISPRi CD73KD) or a non-targeting control
673 sgRNA (J-Lat A72 CRISPRi NT). SgRNA design was conducted using the CRISPick-
674 tool developed by the Broad Institute[85] and sgRNA cloning was performed
675 following the detailed protocol provided by Heckl et al. (2014)[86]. Primer sequences
676 for qPCR and sgRNA cloning are given below.

677 Table 1: Primers for the generation of CRISPRi cell lines.

qPCR	
dCas9 fw	GGATCGAAGAGGGCATCAAA
dCas9 rv	GTTCCTGGTCCACGTACATATC
sgRNA cloning	
CD73 fw	CACCGCGTGAACTGGGTGCGAAAG
CD73 rv	AAACCTTTCGCACCCAGTTCACGC
NT fw	CACC GTATTACTGATATTGGTGGG
NT rv	AAAC CCCACCAATATCAGTAATAC

678

679 **J-Lat cell latency reversal.** J-Lat 5A8 cells (seeded at $1x10^6$ cells/ml) were
680 incubated with CGS21680 (Sigma-Aldrich, Cat. #C141-5MG) or SCH-58261 (Sigma-

681 Aldrich, Cat. #S4568-5MG) at 37°C for 1h at increasing doses in RPMI+/+, followed
682 by stimulation with 20 nM PMA / 1 µM Ionomycin (PMA/I, Sigma-Aldrich, Cat.
683 #10634-1MG and Cat. #10634-1MG). Untreated cells or cells treated with 0.5%
684 DMSO (Sigma-Aldrich, Cat. #D2650-100ML) served as negative controls. 7h after
685 PMA/I reactivation, cells were washed 2x with PBS (ThermoFisher, Scientific, Cat.
686 #14190-250) and viral transcriptional activity, reflected by GFP expression was
687 measured using LSR II flow cytometer (BD Biosciences).

688 Analyses of latency reversal in J-Lat A72 CRISPRi CD73KD and J-Lat A72 CRISPRi
689 NT included an additional pre-gating for-RFP positive cells to specifically select for
690 KD cells prior to the quantification of GFP expression.

691 **Leucocyte isolation and primary CD4+ T cell culture.** Peripheral blood
692 mononuclear cells (PBMCs) from HIV-seronegative donors (Vitalant) were isolated
693 by Ficoll-Hypaque density gradient centrifugation (Corning, Inc., Cat. #25-072-CI)
694 at 2000 rpm (~ 850 x g) at RT for 30 min, without brake. PBMCs were immediately
695 processed to isolate CD4+ T cells by negative selection using the EasySep Human
696 CD4+ T Cell Isolation Cocktail (StemCell Technologies, Cat. #17952) according to
697 manufacturer's protocol. Purified CD4+ T cells were cultured in RPMI+/+.

698 **CD4+ T cell culture under hypoxic conditions.** Following CD4+ T cell isolation,
699 cells were activated with with αCD3/αCD28 activating beads (ThermoFisher
700 Scientific, Cat. #11132D) for 48h at a concentration of 1 bead/cell in the presence
701 of 100 U/ml IL-2 (PeproTech, Inc., Cat. #200-02) in RPMI +/+ and were
702 subsequently cultured under hypoxia (HOX - 1% O_2; Ruskinn Invivo 400
703 workstation), standard conditions (normoxia - NOX - 21% O_2), or were treated with
704 500 µM DMOG (Sigma-Aldrich, Cat. #D3695) up to 5 days post stimulation.

705 **CD4+ T cell *in vitro* infection.** CD4+ T cells were stimulated as described above
706 for 3 days (initial seeding concentration $1x10^6$ cells/ml). At the day of infection,
707 cells were spinoculated in 96-well V-bottom plates (MilliporeSigma, Cat. #M9686-

708 100EA) in 50 µl RPMI+/+ with 100 ng (HIV_{DFII}) of p24 per 1×10^6 cells with 5×10^6
709 cells total per well for 2 h at 2350 rpm (1173 × g) at 37°C. After spinoculation, all
710 cells were returned to culture in the presence of 30 U/ml IL-2. Pre-stimulated CD4+
711 T cells stayed in αCD3/αCD28 activating beads during spininfection and
712 subsequent cell culture. For experiments mimicking hypoxic conditions, cells were
713 treated with 500 µM DMOG (Sigma-Aldrich, Cat. #D3695) or mock-treated with
714 0.5% DMSO two days after αCD3/αCD28 bead stimulation and 24h before HIV_{DFII}
715 spininfection. Cells were kept in DMOG containing RPMI+/+, in presence of
716 activation beads and IL-2 until sample collection 4 days post infection.

717 **CD4+ T cell *in vitro* infection and latency reversal.** Initially, CD4+ T cells were
718 isolated from peripheral blood as described above and subjected to FACS of
719 CD73+ and CD73- cells. To that aim, cells were stained with APC anti-human CD73
720 (BioLegend, Cat. #344006) diluted in PBS (1:20) in 100 µl final volume for 20 min at
721 RT. Cells were then washed twice with PBS and resuspended in 500 µl – 1000 µl
722 PBS to achieve high cell concentrations (20 - $40x10^6$ cells/ml) for FACS. Cells were
723 sorted into 15 ml conical tubes containing 1.5 ml RPMI+/+. Cells were cultured for
724 24h, then infected and rested in the presence of ART to establish *in vitro* latency[47].
725 Briefly, 100 ng of purified NL4-3-Luciferase was added per $1x10^5$ sorted cells, which
726 were then infected by spinoculation as described above. 24h post virus exposure,
727 5 µM saquinavir (protease inhibitor, Sigma-Aldrich, Cat. #S8451-50MG) was added
728 to the cell cultures to suppress spreading infection. 5 days later, cells were
729 stimulated with αCD3/αCD28 beads (or left untreated) in the presence of 30 µM
730 raltegravir (integrase inhibitor, Sigma-Aldrich, Cat. #CDS023737-25MG) to prevent
731 new infections. 24h after stimulation, luciferase activity was quantified using the
732 bright glo luciferase assay system (Promega, Cat. #E2610).

733 **CD4+ T cell staining and processing.** Freshly isolated CD4+ T cells were stained
734 for viability, using the fixable Zombie viability dye (1:100; BioLegend, Cat. #423113)
735 according to the manufacturer's protocol. Subsequently, antibodies APC anti-

736 Human CD73 (1:50), APC-Cy7 anti-Human CD25 (1:100, BD Pharmingen Cat.
737 #557753), and V450 anti-Human CD69 (1:100, BD Horizon Cat. #560740) for cell
738 surface staining diluted in PBS were added and incubated for 20 min at RT. For flow
739 cytometry, cells were washed and fixed in 1% paraformaldehyde (PFA) in PBS after
740 the staining. FACS experiments to isolate populations of interest were performed
741 with live, unfixed cell samples. Flow cytometry analyses were performed on the LSR
742 II flow cytometer (BD Biosciences) or MA900 Multi-Application Cell Sorter (Sony
743 Biotechnologies). All fluorescent-based sorts were conducted on the latter
744 instrument.

745 **Immunophenotyping of CD4+ T cells from HIV-infected individuals.** 30 mLs
746 of fresh blood were obtained from each of six HIV-positive individuals on long-
747 term continuous ART (greater than one year) who were stably suppressed (HIV
748 RNA <40 copies/mL); samples were processed as described above. Purified CD4+
749 T cells were then stained using a panel of antibodies against previously described
750 reservoir markers (see Table 2), as well as CD4, CD73, CD39 and a live/dead staining
751 (ThermoFisher Cat. #L34961). Finally, cells were subjected to flow cytometry
752 measurement on a Cytek Aurora (5L) instrument.

753 Table 2: Antibody panel used to phenotype CD4+ T cells from HIV-infected individuals.

Specificity	fluorophore	Manufacturer	Cat. #
CD4	BUV395	BD Biosciences	564724
CD30	BV421	BD Biosciences	566253
CD32	PerCP/Cy5.5	BioLegend	303215
CD20	BV605	BioLegend	302333
CD2	BV510	BioLegend	300217
CD279 (PD-1)	PE	BioLegend	329905
CD49d	BUV737	BD Biosciences	612850
CD39	PE-Cy7	BioLegend	329905
CD98	FITC	BioLegend	315603
CTLA-4	BV785	BioLegend	369623

754

755 **Flow cytometry gating and data analysis.** Data were analyzed and visualized
756 using the FlowJo software (v.10.7.1). Crosstalk compensations was performed using
757 single-stained samples for each of the fluorochromes and isotype controls were
758 employed to assess antigen positivity and enable specific gating. FACS and flow
759 cytometry gating was performed as follows: low/negative cells for live/dead dyes
760 were selected for single cells and subsequent FSC/SSC scatter plots. Then, antibody
761 gates were defined based on suited /single stained and isotype controls. Gating of
762 HIV_{DFII} reporter expression was based on non-infected, mock-treated (*in vitro*
763 activated) negative control samples to account for activation-dependent increase
764 of cellular background fluorescence.

765 **Expression Profiling via NanoString.** Quantitative RNA and protein expression
766 data were generated using the nCounter Vantage 3D RNA:Protein Immune Cell
767 Profiling Assay (NanoString Technologies, Inc., Cat. #121100019) and the nCounter
768 SPRINT profiler (NanoString Technologies), comprising 770 RNA and 30 protein
769 targets as well as positive and negative controls. 100,000 viable, sorted cells were
770 used per sample, which were processed according to the manufacturer's
771 instructions. RNA and protein expression values were normalized and analyzed
772 using the nSolver Analysis Software 4.0 and the add-on Advanced Analysis
773 Software 2.0.115 (NanoString Technologies). Samples that did not pass the default
774 control performance and quality parameters were excluded from subsequent
775 analysis. Normalization genes for each sample were automatically selected by the
776 software based on the geNorm algorithm. Biological replicates were grouped
777 according to sample type and the differential expression of each analyte-type (RNA
778 or protein target) was determined in cross-comparisons among all sample types
779 by considering inter-donor differences as confounding variable unless otherwise
780 stated. Intersections of significant targets of individual differential expression
781 analyses were visualized in a Venn diagram using an open source platform from
782 Bioinformatics & Evolutionary Genomics[87].

783 Based on the differential expression of each gene, gene sets pre-defined by
784 nanoString, representing different pathways included in this assay, were analyzed
785 by calculating global significance scores for each gene set within each sample as
786 follows: undirected global significance statistic = $\left(\frac{1}{p}\sum_{i=1}^{p} t_i^2\right)^{\frac{1}{2}}$, where ti is the t-
787 statistic from the ith pathway gene. The directed global significance statistic is
788 similar to the undirected global significance statistic, but rather than measuring the
789 tendency of a pathway to have differentially expressed genes, it measures the
790 tendency to have over- or under-expressed genes. It is calculated similarly to the
791 undirected global significance score, but it takes the sign of the t-statistics into
792 account: Directed global significance statistic = $sign(U)|U|^{1/2}$ where U =
793 $\left(\frac{1}{p}\sum_{i=1}^{p} sign(t_i) * t_i^2\right)$ and where sign(U) equals -1 if U is negative and 1 if U is
794 positive (MAN-10030-02[88]).

795 **CyTOF samples preparation and analysis**. For live/dead discrimination, 0.1-1
796 million cells per sample were treated with cisplatin (Sigma-Aldrich) and fixed with
797 paraformaldehyde (PFA) as previously described[9,28,29]. Briefly, Cells were washed
798 once with contaminant-free PBS (Rockland) with 2 mM EDTA (Corning), centrifuged
799 and resuspend with 25 μM cisplatin in 4 ml PBS/EDTA and incubated for 60 seconds
800 at room temperature, and then quenched with CyFACS (metal contaminant-free
801 PBS supplemented with 0.1% bovine serum albumin and 0.1% sodium azide). Cells
802 were then centrifuged, fixed with 2% PFA in metal contaminant-free PBS and
803 washed 3x with CyFACS. These fixed cells were stored at -80°C until CyTOF
804 staining.

805 Prior to CyTOF staining, multiple samples were barcoded using the Cell-ID 20-Plex
806 Pd Barcoding Kit according to manufacturer's instructions (Fluidigm). Briefly, each
807 sample was washed twice with Barcode Perm buffer (Fluidigm), and incubated for
808 30 min with the appropriate barcode at a 1:90 ratio. Cells were then washed with
809 0.8 ml Maxpar Cell Staining buffer (Fluidigm) in Nunc™ 96 Deep-Well polystyrene

810 plates (Thermo Fisher), followed by CyFACS. Barcoded samples were combined and
811 blocked with sera from mouse (Thermo Fisher), rat (Thermo Fisher), and human (AB
812 serum, Sigma-Aldrich) for 15 minutes at 4°C. Cells were washed twice with CyFACS
813 buffer and stained with the cocktail of CyTOF surface staining antibodies (Table S1)
814 for 45 min on ice. Subsequently, cells were washed 3X with CyFACS buffer and fixed
815 overnight at 4°C with 2% PFA (Electron Microscopy Sciences) in metal
816 contaminant-free PBS. For intracellular staining, cells were permeabilized by
817 incubation with fix/perm buffer (eBioscience) for 30 min at 4°C and washed twice
818 with Permeabilization Buffer (eBioscience). Cells were blocked again with sera from
819 mouse and rat for 15 min on ice, washed twice with Permeabilization Buffer
820 (eBioscience), and stained with the cocktail of CyTOF intracellular staining
821 antibodies (Table S1) for 45 min on ice. Cells were then washed once with CyFACS
822 and incubated for 20 min at room temperature with 250 nM Cell-IDTM DNA
823 Intercalator-Ir (Fluidigm) in 2% PFA diluted in PBS. Cells were washed twice with
824 CyFACS, once with Maxpar Cell Staining Buffer (Fluidigm), once with Maxpar PBS
825 (Fluidigm), and once with Maxpar Cell Acquisition Solution (CAS, Fluidigm).
826 Immediately prior to acquisition, cells were resuspended in EQTM calibration beads
827 (Fluidigm) diluted in CAS. Cells were acquired at a rate of 250-350 events/sec on a
828 CyTOF2 instrument (Fluidigm) at the UCSF Parnassus single cell analysis facility.

829 Data were normalized to EQTM calibration beads and de-barcoded with CyTOF
830 software (Fluidigm). Normalized data were imported into FlowJo (BD) for gating
831 (cell, intact, live, single events) and heatmap was generated in Cytobank.

832 **RNA Sequencing.** Freshly isolated CD4+ T cells from healthy blood donors were
833 sorted based on their CD73 expression as described above. $3x10^6$ cells were
834 collected per sample and stored as dry cell pellets at -80 °C. RNA preparation,
835 library preparation and mRNA sequencing were conducted at Genewiz (USA).
836 Paired-end sequencing was performed using the Illumina NovaSeq 6000
837 instrument to obtain a minimum of 20 million read pairs per sample with a read

838 length of 2x150 bp. Sequence reads were trimmed to remove possible adapter
839 sequences and nucleotides with poor quality using Trimmomatic v.0.36. The
840 trimmed reads were mapped to the Homo sapiens GRCh38 reference genome
841 available on ENSEMBL using the STAR aligner v.2.5.2b. Unique gene hit counts were
842 calculated by using featureCounts from the Subread package v.1.5.2. The hit counts
843 were summarized and reported using the gene_id feature in the annotation file.
844 Only unique reads that fell within exon regions were counted. After extraction of
845 gene hit counts, the gene hit counts table was used for downstream differential
846 expression analysis. Using DESeq2, a comparison of gene expression between
847 samples was performed adjusting for the donor effect as confounding variable. The
848 Wald test was used to generate p-values and $\log_2$ fold changes. Genes with an
849 adjusted p-value < 0.05 (Benjamini-Hochberg method) and absolute $\log_2$ fold
850 change > 1 were called as differentially expressed genes for each comparison. A
851 gene ontology analysis was performed on the statistically significant set of genes
852 by implementing the software GeneSCF v.1.1-p2. The goa_human GO list was used
853 to cluster the set of genes based on their biological processes and determine their
854 statistical significance. A list of genes clustered based on their gene ontologies was
855 generated.

856

857 ***In Situ* Detection of HIV and Cellular Markers.** The experimental procedure for
858 the in situ and immunofluorescence staining has been described in detail in
859 previous publications[52,53]. The assay enables the detection of HIV-integrated DNA,
860 viral mRNA, viral proteins, and several cellular markers in the same assay. Sample
861 preparation, data acquisition and subsequent analyses were conducted in the
862 laboratory of Dr. Eliseo Eugenin (UTMB, Texas).

863 **Tissue samples.** Tissues from ART-suppressed individuals who have been on
864 treatment for at least 6 months and had viral loads below clinical detection limits

865 (<50 RNA copies/ml), as well as tissues from HIV-negative and ART-naïve viremic
866 individuals with high plasma loads (>50 RNA copies/ml) were part of an ongoing
867 research protocol approved by University of Texas Medical Branch (UTMB). Further
868 clinical data and additional information are available and will be provided upon
869 request by the lead contact Eliseo Eugenin (eleugeni@utmb.edu). All tissues were
870 obtained with full, written consent from the study participants and freshly collected
871 specimens were immediately fixed with 4% PFA, then mounted into paraffin blocks,
872 subjected to tissue sectioning, and ultimately to ab analysis by *in situ* and
873 immunostaining.

874 **Staining procedures.** Paraffin-embedded slides containing the tissue samples
875 were consecutively immersed in the following solutions: xylene for 5 min (2 times),
876 100% EtOH for 3 min, 100% EtOH for 3 min, 95% EtOH for 3 min, 90% EtOH for 3
877 min, 70% EtOH for 3 min, 60% EtOH for 3 min, 50% EtOH for 3 min, miliQ H_2O for
878 3 min. Then, tissue was encircled with ImmEdge Pen to reduce the reagent volume
879 needed to cover the specimens. Finally, slides were immersed in miliQ H_2O for 3
880 min. For Protein K treatment, tissues were incubated with proteinase K diluted 1:10
881 in 1X TBS (Fisher Scientific, Cat. #BP24711; and PNA ISH kit, Agilent Dako, Cat.
882 #K5201) for 10 min at RT in a humidity chamber. Next, slides were immersed in
883 miliQ H2O for 3 min, then immersed in 95% EtOH for 20 sec and finally, the slides
884 were left air-dry for 5 min. For HIV DNA probe hybridization tissues were incubated
885 with 10 μM PNA DNA probe for Nef-PNA Alexa Fluor 488 and Alu-PNA Cy5 (PNA
886 Bio). Next, slides were placed in a pre-warmed humidity chamber and incubated at
887 42°C for 30 min, then the temperature was raised to 55°C for an additional 1 h
888 incubation. Subsequently, tissues were incubated using Preheat Stringent Wash
889 working solution (PNA ISH kit) diluted 1:60 in 1X TBS for 25 min in an orbital shaker
890 at 55°C. Slides were equilibrated to RT by brief immersion in TBS for 20 sec. HIV
891 mRNA detection followed the manufacturer's protocol for RNAscope 2.5 HD
892 Detection Reagent-RED (Advanced Cell Diagnostics, Inc., Cat. #322360). Probe for

893 HIV Gag-pol was added to the tissue samples and incubated for 30 min at 42°C
894 and then 50 min at 55°C. Next, samples were incubated in Preheat Stringent Wash
895 working solution diluted 1:60 in 1X TBS (PNA ISH kit) for 15 min in an orbital shaker
896 at 55°C. Finally, slides were immersed in 1X TBS for 20 sec. For HIV or cellular
897 protein detection, antigen retrieval was performed by incubating slide sections in
898 commercial antigen retrieval solution (Agilent Dako, Cat. #S1700) for 30 min in a
899 water-bath at 80°C. Next, slides were removed from the bath and cooled down in
900 1X TBS. Samples were permeabilized with 0.1% Triton X-100 (Sigma-Aldrich, Cat.
901 #X100) for 2 min and then washed in 1X TBS for 5 min three times. Unspecific
902 antibody binding sites were blocked by incubating samples with a freshly prepared
903 blocking solution. Afterwards, sections were incubated overnight at 4°C using a
904 humidity chamber (10 ml of blocking solution: 1 mL 0.5 M EDTA, 100 ul Fish Gelatin
905 from cold water 45%, 0.1 g Albumin from Bovine serum Fraction V, 100 ul horse
906 serum, 5% human serum, 9 mL miliQ H_2O). Anti-p24 primary antibodies were
907 added to the samples diluted in a blocking solution and incubated at 4°C
908 overnight. To perform these analyses, large amounts of antibodies (obtained from
909 the NIH AIDS repository) were purified and pre-absorbed in uninfected human
910 tissues as well as tested in cell lines to assure specificity and proper binding to the
911 target (see Donoso et al.[52] for details). Following antibody staining, slides were
912 washed in 1X TBS 5 min for three times to eliminate unbound antibodies.
913 Secondary antibodies were added at the appropriate dilutions and incubated for
914 2h at RT. Slides were washed three times in 1X TBS for 5 min to eliminate unbound
915 antibodies. Next, slides were mounted using Prolong Diamond Antifade Mount
916 medium containing DAPI (ThermoFisher Scientific, Cat. #P36931). Slides were kept
917 in the dark at 4°C.

918 **Image acquisition and analysis.** Cells were examined by confocal microscopy
919 using an A1 Nikon confocal microscope with spectral detection and unmixing
920 systems. Image analysis was performed using the Nikon NIS Elements Advanced

921 Research imaging software (Nikon Instruments, Japan). The automated image
922 segmentation and analysis are based on the following premises: For detection of
923 HIV-integrated DNA, first, automatic or manual detection of cells that are positive
924 for HIV-DNA and second, the HIV-DNA probe has to colocalize with DAPI and Alu
925 repeats staining with a Pearson's correlation coefficient of at least 0.8 as described
926 previously[89]. These two conditions are essential for HIV-integrated DNA, or the
927 signal is considered negative or unspecific. For detection of HIV-mRNA, first, low
928 colocalization with DAPI or Alu-repeats (0.2 Pearson's correlation coefficient or
929 below) and second, presence in cells with HIV-DNA signal. The sensitivity, accuracy
930 and specificity of the system were previously validated in the laboratory of our
931 collaborator in two well characterized T cell lines A3.01 (uninfected) and ACH-2
932 (HIV-infected) and two monocytic cell lines, HL-60 (uninfected) and OM-10 (HIV-
933 infected).

934 To analyze local microenvironments of CD3+ cells, CD73 expression was assessed
935 in cell neighborhoods by lineplot analysis. Image segmentation and quantification
936 were performed using Nikon NIS Elements Advanced Research imaging software
937 (Nikon Instruments, Japan) and Ilastik[90]. CD73 signals were analyzed along straight
938 lines of 80 µM length, placing the zero point at the center of the line, at the position
939 of the respective CD3-positive cell. Obtained CD73 intensities were normalized to
940 the mean CD73 intensity in CD3+ HIV-DNA-/p24+ (ART suppr.) samples (see
941 Figure S7).

942 **Quantification and Statistical Analysis.** Statistical details are given in the figure
943 legends. All statistical analyses were performed using GraphPad Prism software
944 version 9. P-values ≤ 0.05 were considered statistically significant. A Student's two-
945 tailed t-test was used for two-way column analyses. ANOVA tests were used for
946 multiple comparisons. P-values are denoted in the figure panels. Data are
947 presented as means with error bars indicating the standard error of the mean (SEM)
948 unless otherwise stated.

949

DATA AVAILABILITY

The datasets generated and/or analyzed during the current study are available from the corresponding author on reasonable request.

ACKNOWLEDGEMENTS

The authors would like to acknowledge Guorui Xie, PhD and Ashley George, PhD for helpful input regarding the CyTOF analysis. The authors thank Leonard Chavez, PhD and Shivani Desai for providing reagents, Vivienne Schneider for experimental support, as well as Konstantinos Georgiou, PhD and Zain Y. Dossani, PhD for guidance and support in data analysis. The authors sincerely thank Rebecca Hoh for her help in obtaining clinical specimens for our study.

This study was supported by National Institutes of Health (NIH) grants R01AI150449 and R01MH112457 (to S.K.P.). We would like to thank The National NeuroAIDS Tissue Consortium (NNTC) for providing all human samples and associated information. The NNTC is made possible through funding from the NIMH and NINDS by the following grants: Manhattan HIV Brain Bank (MHBB): U24MH100931; Texas NeuroAIDS Research Center (TNRC): U24MH100930; National Neurological AIDS Bank (NNAB): U24MH100929; California NeuroAIDS Tissue Network (CNTN): U24MH100928; and Data Coordinating Center (DCC); R01AI147777; R01AI127219; UM1AI64567; UM1AI64559. The staining and analysis were funded by the National Institute of Mental Health grant, MH096625 and MH128032 and the National Institute of Neurological Disorders and Stroke, NS105584 (to E. A. E.).

COMPETING INTERESTS

The authors declare no competing financial or non-financial interests.

974 **REFERENCES**

975 1. Ho, Y.-C. *et al.* Replication-Competent Noninduced Proviruses in the Latent
976 Reservoir Increase Barrier to HIV-1 Cure. *Cell* **155**, 540–551 (2013).
977 2. Davey, R. T. *et al.* HIV-1 and T cell dynamics after interruption of highly active
978 antiretroviral therapy (HAART) in patients with a history of sustained viral
979 suppression. *Proc. Natl. Acad. Sci. U. S. A.* **96**, 15109–15114 (1999).
980 3. Finzi, D. *et al.* Latent infection of CD4+ T cells provides a mechanism for lifelong
981 persistence of HIV-1, even in patients on effective combination therapy. *Nat.*
982 *Med.* **5**, 512–517 (1999).
983 4. Siliciano, J. D. & Siliciano, R. F. *Latency and viral persistence in HIV-1 infection*.
984 *The Journal of Clinical Investigation* vol. 106 (2000).
985 5. Chun, T.-W. W. *et al.* Quantification of latent tissue reservoirs and total body
986 viral load in HIV-1 infection. *Nature* **387**, 183–188 (1997).
987 6. Finzi, D. *et al.* Identification of a reservoir for HIV-1 in patients on highly active
988 antiretroviral therapy. *Science* **278**, 1295–1300 (1997).
989 7. Wong, J. K. *et al.* Recovery of replication-competent HIV despite prolonged
990 suppression of plasma viremia. *Science* **278**, 1291–1295 (1997).
991 8. WM, E.-S. *et al.* CD4+ Count–Guided Interruption of Antiretroviral Treatment.
992 *N. Engl. J. Med.* **355**, 2283–2296 (2006).
993 9. Neidleman, J. *et al.* Phenotypic analysis of the unstimulated in vivo hiv cd4 t cell
994 reservoir. *eLife* **9**, 1–34 (2020).
995 10. Kulpa, D. A. & Chomont, N. HIV persistence in the setting of antiretroviral
996 therapy: when, where and how does HIV hide? *J. Virus Erad.* **1**, 59–66 (2015).
997 11. Darcis, G., Berkhout, B. & Pasternak, A. O. The quest for cellular markers of HIV
998 reservoirs: Any color you like. *Front. Immunol.* **10**, 2251 (2019).
999 12. Fromentin, R. *et al.* CD4+ T Cells Expressing PD-1, TIGIT and LAG-3 Contribute
1000 to HIV Persistence during ART. *PLoS Pathog.* **12**, (2016).

1001 13. McGary, C. S. *et al.* CTLA-4+PD-1− Memory CD4+ T Cells Critically Contribute
1002 to Viral Persistence in Antiretroviral Therapy-Suppressed, SIV-Infected Rhesus
1003 Macaques. *Immunity* **47**, 776-788.e5 (2017).
1004 14. Iglesias-Ussel, M., Vandergeeten, C., Marchionni, L., Chomont, N. & Romerio, F.
1005 High Levels of CD2 Expression Identify HIV-1 Latently Infected Resting Memory
1006 CD4+ T Cells in Virally Suppressed Subjects. *J. Virol.* **87**, 9148–9158 (2013).
1007 15. Serra-Peinado, C. *et al.* Expression of CD20 after viral reactivation renders HIV-
1008 reservoir cells susceptible to Rituximab. *Nat. Commun.* **10**, 1–15 (2019).
1009 16. Hogan, L. E. *et al.* Increased HIV-1 transcriptional activity and infectious burden
1010 in peripheral blood and gut-associated CD4+ T cells expressing CD30. *PLOS*
1011 *Pathog.* **14**, e1006856 (2018).
1012 17. Descours, B. *et al.* CD32a is a marker of a CD4 T-cell HIV reservoir harbouring
1013 replication-competent proviruses. *Nature* **543**, 564–567 (2017).
1014 18. Pérez, L. *et al.* Conflicting evidence for HIV enrichment in CD32+ CD4 T cells.
1015 *Nature* **561**, E9–E16 (2018).
1016 19. Osuna, C. E. *et al.* Evidence that CD32a does not mark the HIV-1 latent reservoir.
1017 *Nature* **561**, E20–E28 (2018).
1018 20. Martin, G. E. *et al.* CD32-expressing CD4 T cells are phenotypically diverse and
1019 can contain proviral HIV DNA. *Front. Immunol.* **9**, 1 (2018).
1020 21. Thornhill, J. P. *et al.* CD32 expressing doublets in HIV-infected gut-associated
1021 lymphoid tissue are associated with a T follicular helper cell phenotype.
1022 *Mucosal Immunol.* **12**, 1212–1219 (2019).
1023 22. Noto, A. *et al.* CD32 + and PD-1 + Lymph Node CD4 T Cells Support Persistent
1024 HIV-1 Transcription in Treated Aviremic Individuals. *J. Virol.* **92**, 901–919 (2018).
1025 23. Vasquez, J. J. *et al.* CD32-RNA Co-localizes with HIV-RNA in CD3+ Cells Found
1026 within Gut Tissues from Viremic and ART-Suppressed Individuals. *Pathog.*
1027 *Immun.* **4**, 147 (2019).

1028 24. Adams, P. *et al.* CD32+CD4+ memory T cells are enriched for total HIV-1 DNA
1029 in tissues from humanized mice. *iScience* **24**, (2020).
1030 25. Darcis, G. *et al.* CD32+CD4+ T Cells Are Highly Enriched for HIV DNA and Can
1031 Support Transcriptional Latency. *Cell Rep.* **30**, 2284-2296.e3 (2020).
1032 26. Calvanese, V., Chavez, L., Laurent, T., Ding, S. & Verdin, E. Dual-color HIV
1033 reporters trace a population of latently infected cells and enable their
1034 purification. *Virology* **446**, 283–292 (2013).
1035 27. Chavez, L., Calvanese, V. & Verdin, E. HIV Latency Is Established Directly and
1036 Early in Both Resting and Activated Primary CD4 T Cells. *PLOS Pathog.* **11**,
1037 e1004955 (2015).
1038 28. Ma, T. *et al.* HIV efficiently infects T cells from the endometrium and remodels
1039 them to promote systemic viral spread. *eLife* **9**, 1–24 (2020).
1040 29. Xie, G. *et al.* Characterization of HIV-induced remodeling reveals differences in
1041 infection susceptibility of memory CD4 + T cell subsets in vivo. *Cell Rep.* **35**,
1042 (2021).
1043 30. Kerkau, T., Gernert, S., Kneitz, C. & Schimpl, A. Mechanism of MHC Class I
1044 Downregulation in HIV Infected Cells. *Immunobiology* **184**, 402–409 (1992).
1045 31. Cohen, G. B. *et al.* The selective downregulation of class I major
1046 histocompatibility complex proteins by HIV-1 protects HIV-infected cells from
1047 NK cells. *Immunity* **10**, 661–671 (1999).
1048 32. Jacobs, M. D. & Harrison, S. C. Structure of an IκBα/NF-κB complex. *Cell* **95**,
1049 749–758 (1998).
1050 33. Ruelas, D. S. & Greene, W. C. An Integrated Overview of HIV-1 Latency. *Cell*
1051 **155**, 519–529 (2013).
1052 34. Greene, W. C. & Peterlin, B. M. Charting HIV's remarkable voyage through the
1053 cell: Basic science as a passport to future therapy. *Nat. Med.* **8**, 673–680 (2002).
1054 35. Doitsh, G. *et al.* Cell death by pyroptosis drives CD4 T-cell depletion in HIV-1
1055 infection. *Nature* **505**, 509–514 (2014).

1056 36. Allard, B., Allard, D., Buisseret, L. & Stagg, J. The adenosine pathway in immuno-
1057 oncology. *Nat. Rev. Clin. Oncol.* **17**, 611–629 (2020).
1058 37. Kazemi, M. H. *et al.* Adenosine and adenosine receptors in the
1059 immunopathogenesis and treatment of cancer. *J. Cell. Physiol.* **233**, 2032–2057
1060 (2018).
1061 38. Di Virgilio, F. & Adinolfi, E. Extracellular purines, purinergic receptors and tumor
1062 growth. *Oncogene* **36**, 293–303 (2017).
1063 39. Yegutkin, G. G., Henttinen, T., Samburski, S. S., Spychala, J. & Jalkanen, S. *The*
1064 *evidence for two opposite, ATP-generating and ATP-consuming, extracellular*
1065 *pathways on endothelial and lymphoid cells*. *Biochem. J* vol. 367 121–128
1066 (2002).
1067 40. Antonioli, L., Pacher, P., Vizi, E. S. & Haskó, G. CD39 and CD73 in immunity and
1068 inflammation. *Trends Mol. Med.* **19**, 355–367 (2013).
1069 41. Hansen, K. R., Resta, R., Webb, C. F. & Thompson, L. F. Isolation and
1070 characterization of the promoter of the human 5′-nucleotidase (CD73)-
1071 encoding gene. *Gene* **167**, 307–312 (1995).
1072 42. Fausther, M., Sheung, N., Saiman, Y., Bansal, M. B. & Dranoff, J. A. Activated
1073 hepatic stellate cells upregulate transcription of ecto-5=-nucleotidase/ CD73
1074 via specific SP1 and SMAD promoter elements. *Am J Physiol Gastrointest Liver*
1075 *Physiol* **303**, 904–914 (2012).
1076 43. Synnestvedt, K. *et al.* Ecto-5′-nucleotidase (CD73) regulation by hypoxia-
1077 inducible factor-1 mediates permeability changes in intestinal epithelia. *J. Clin.*
1078 *Invest.* **110**, 993–1002 (2002).
1079 44. Kordaß, T., Osen, W. & Eichmüller, S. B. Controlling the immune suppressor:
1080 Transcription factors and MicroRNAs regulating CD73/NT5E. *Front. Immunol.*
1081 **9**, 813 (2018).

1082 45. Towatari, M., Kanei, Y., Saito, H. & Hamaguchi, M. Hematopoietic transcription
1083 factor GATA-2 activates transcription from HIV-1 long terminal repeat. *AIDS* **12**,
1084 253–259 (1998).
1085 46. Balakrishna, S. L., Satyanarayana, N. & Kondapi, A. K. Involvement of human
1086 topoisomerase II isoforms in HIV-1 reverse transcription. *Arch. Biochem.*
1087 *Biophys.* **532**, 91–102 (2013).
1088 47. Lassen, K. G., Hebbeler, A. M., Bhattacharyya, D., Lobritz, M. A. & Greene, W. C.
1089 A Flexible Model of HIV-1 Latency Permitting Evaluation of Many Primary CD4
1090 T-Cell Reservoirs. *PLoS ONE* **7**, e30176 (2012).
1091 48. Jordan, A. HIV reproducibly establishes a latent infection after acute infection
1092 of T cells in vitro. *EMBO J.* **22**, 1868–1877 (2003).
1093 49. Chan, J. K., Bhattacharyya, D., Lassen, K. G., Ruelas, D. & Greene, W. C.
1094 Calcium/Calcineurin Synergizes with Prostratin to Promote NF-κB Dependent
1095 Activation of Latent HIV. *PLoS ONE* **8**, e77749 (2013).
1096 50. Lamers, S. L. *et al.* HIV DNA Is Frequently Present within Pathologic Tissues
1097 Evaluated at Autopsy from Combined Antiretroviral Therapy-Treated Patients
1098 with Undetectable Viral Loads. *J. Virol.* **90**, 8968–8983 (2016).
1099 51. Prevedel, L. *et al.* Identification, Localization, and Quantification of HIV
1100 Reservoirs Using Microscopy. *Curr. Protoc. Cell Biol.* **82**, 64 (2019).
1101 52. Donoso, M. *et al.* Identification, Quantification, and Characterization of HIV-1
1102 Reservoirs in the Human Brain. (2022) doi:10.3390/cells11152379.
1103 53. D'Amico, D. *et al.* Chronic brain damage in HIV-infected individuals under
1104 antiretroviral therapy is associated with viral reservoirs, sulfatide release, and
1105 compromised cell-to-cell communication. *Cell. Mol. Life Sci. CMLS* **80**, 116
1106 (2023).
1107 54. Carreau, A., Hafny-Rahbi, B. E., Matejuk, A., Grillon, C. & Kieda, C. Why is the
1108 partial oxygen pressure of human tissues a crucial parameter? Small molecules
1109 and hypoxia. *J. Cell. Mol. Med.* **15**, 1239–1253 (2011).

1110 55. Zenewicz, L. A. Oxygen Levels and Immunological Studies. *Front. Immunol.* **8**,
1111 8–11 (2017).
1112 56. Caldwell, C. C. *et al.* Differential Effects of Physiologically Relevant Hypoxic
1113 Conditions on T Lymphocyte Development and Effector Functions. *J. Immunol.*
1114 **167**, 6140–6149 (2001).
1115 57. Ohta, A. *et al.* In vivo T cell activation in lymphoid tissues is inhibited in the
1116 oxygen-poor microenvironment. *Front. Immunol.* **2**, (2011).
1117 58. Charles, S. *et al.* Regulation of HIV-1 transcription at 3% versus 21% oxygen
1118 concentration. *J. Cell. Physiol.* **221**, 469–479 (2009).
1119 59. Deshmane, S. L., Amini, S., Sen, S., Khalili, K. & Sawaya, B. E. Regulation of the
1120 HIV-1 promoter by HIF-1α and Vpr proteins. *Virol. J.* **8**, 477 (2011).
1121 60. Deshmane, S. L. *et al.* Activation of the Oxidative Stress Pathway by HIV-1 Vpr
1122 Leads to Induction of Hypoxia-inducible Factor 1α Expression. *J. Biol. Chem.*
1123 **284**, 11364–11373 (2009).
1124 61. Duette, G. *et al.* Induction of HIF-1α by HIV-1 Infection in CD4 + T Cells
1125 Promotes Viral Replication and Drives Extracellular Vesicle-Mediated
1126 Inflammation. *mBio* **9**, 1–21 (2018).
1127 62. Zhuang, X. *et al.* Hypoxic microenvironment shapes HIV-1 replication and
1128 latency. *Commun. Biol.* **3**, (2020).
1129 63. Romio, M. *et al.* Extracellular purine metabolism and signaling of CD73-derived
1130 adenosine in murine Treg and Teff cells. *Am. J. Physiol.-Cell Physiol.* **301**, C530–
1131 C539 (2011).
1132 64. Sheridan, C. M., Heist, E. K., Beals, C. R., Crabtree, G. R. & Gardner, P. Protein
1133 kinase A negatively modulates the nuclear accumulation of NF-ATc1 by priming
1134 for subsequent phosphorylation by glycogen synthase kinase-3. *J. Biol. Chem.*
1135 **277**, 48664–48676 (2002).
1136 65. D'Alessandro, S. *et al.* Effect of Hypoxia on Gene Expression in Cell Populations
1137 Involved in Wound Healing. *BioMed Res. Int.* **2019**, 1–20 (2019).

1138 66. Poth, J. M., Brodsky, K., Ehrentraut, H., Grenz, A. & Eltzschig, H. K. Transcriptional
1139 control of adenosine signaling by hypoxia-inducible transcription factors
1140 during ischemic or inflammatory disease. *J. Mol. Med.* **91**, 183–193 (2013).
1141 67. Tóth, I. *et al.* Decreased frequency of CD73 + CD8 + T cells of HIV-infected
1142 patients correlates with immune activation and T cell exhaustion. *J. Leukoc. Biol.*
1143 **94**, 551–561 (2013).
1144 68. Schuler, P. J. *et al.* CD4+CD73+ T cells are associated with lower T-cell activation
1145 and C reactive protein levels and are depleted in HIV-1 infection regardless of
1146 viral suppression. *AIDS* **27**, 1545–1555 (2013).
1147 69. Wang, X. *et al.* Decreased CD73+ Double-Negative T Cells and Elevated Level
1148 of Soluble CD73 Correlated With and Predicted Poor Immune Reconstitution in
1149 HIV-Infected Patients After Antiretroviral Therapy. *Front. Immunol.* **0**, 1445
1150 (2022).
1151 70. Li, J. *et al.* Reversal of the CD8+ T-Cell Exhaustion Induced by Chronic HIV-1
1152 Infection Through Combined Blockade of the Adenosine and PD-1 Pathways.
1153 *Front. Immunol.* **12**, 1–11 (2021).
1154 71. Nikolova, M. *et al.* CD39/Adenosine Pathway Is Involved in AIDS Progression.
1155 *PLoS Pathog.* **7**, e1002110 (2011).
1156 72. He, T. *et al.* Critical Role for the Adenosine Pathway in Controlling Simian
1157 Immunodeficiency Virus-Related Immune Activation and Inflammation in Gut
1158 Mucosal Tissues. *J. Virol.* **89**, 9616–9630 (2015).
1159 73. Moreno-Fernandez, M. E., Rueda, C. M., Rusie, L. K. & Chougnet, C. A.
1160 Regulatory T cells control HIV replication in activated T cells through a cAMP-
1161 dependent mechanism. *Blood* **117**, 5372–5380 (2011).
1162 74. Li, G. *et al.* Regulatory T Cells Contribute to HIV-1 Reservoir Persistence in CD4
1163 + T Cells Through Cyclic Adenosine Monophosphate-Dependent Mechanisms
1164 in Humanized Mice in Vivo. *J. Infect. Dis.* **216**, 1579–1591 (2017).

1165 75. Seddiki, N. *et al.* CD73 + CD127 high Long-Term Memory CD4 T Cells Are
1166 Highly Proliferative in Response to Recall Antigens and Are Early Targets in HIV-
1167 1 Infection. (2021) doi:10.3390/ijms22020912.
1168 76. Zhang, B. CD73 promotes tumor growth and metastasis. *OncoImmunology* **1**,
1169 67–70 (2012).
1170 77. Chen, S. *et al.* CD73 expression on effector T cells sustained by TGF-β facilitates
1171 tumor resistance to anti-4-1BB/CD137 therapy. *Nat. Commun.* **10**, 1–15 (2019).
1172 78. Vijayan, D. *et al.* Selective activation of anti-CD73 mechanisms in control of
1173 primary tumors and metastases. *OncoImmunology* **6**, e1312044–e1312044
1174 (2017).
1175 79. Allard, D., Chrobak, P., Allard, B., Messaoudi, N. & Stagg, J. Targeting the CD73-
1176 adenosine axis in immuno-oncology. *Immunol. Lett.* 1–9 (2018)
1177 doi:10.1016/j.imlet.2018.05.001.
1178 80. Sek, K. *et al.* Targeting Adenosine Receptor Signaling in Cancer
1179 Immunotherapy. *Int. J. Mol. Sci.* **19**, 3837 (2018).
1180 81. Leone, R. D. & Emens, L. A. Targeting adenosine for cancer immunotherapy. *J.*
1181 *Immunother. Cancer* **6**, 57 (2018).
1182 82. Chen, S. *et al.* CD73: an emerging checkpoint for cancer immunotherapy.
1183 *Immunotherapy* **11**, 983–997 (2019).
1184 83. Antonioli, L., Yegutkin, G. G., Pacher, P., Blandizzi, C. & Haskó, G. Anti-CD73 in
1185 Cancer Immunotherapy: Awakening New Opportunities. *Trends Cancer* **2**, 95–
1186 109 (2016).
1187 84. Zhang, B. CD73: A Novel Target for Cancer Immunotherapy. *Cancer Res.* **70**,
1188 6407–6411 (2010).
1189 85. CRISPick. https://portals.broadinstitute.org/gppx/crispick/public.
1190 86. Heckl, D. *et al.* Generation of mouse models of myeloid malignancy with
1191 combinatorial genetic lesions using CRISPR-Cas9 genome editing. *Nat.*
1192 *Biotechnol.* **32**, 941–946 (2014).

1193 87. Gent, U. of. Draw Venn Diagram. *Bioinformatics and Evolutionary Genetics*
1194 http://bioinformatics.psb.ugent.be/webtools/Venn/.
1195 88. NanoString Technologies. nCounter Advanced Analysis 2.0 - User Manual.
1196 (2018).
1197 89. Dunn, K. W., Kamocka, M. M. & McDonald, J. H. A practical guide to evaluating
1198 colocalization in biological microscopy. *Am. J. Physiol. Cell Physiol.* **300**, C723–
1199 C742 (2011).
1200 90. Berg, S. *et al.* ilastik: interactive machine learning for (bio)image analysis. *Nat.*
1201 *Methods* **16**, 1226–1232 (2019).
1202